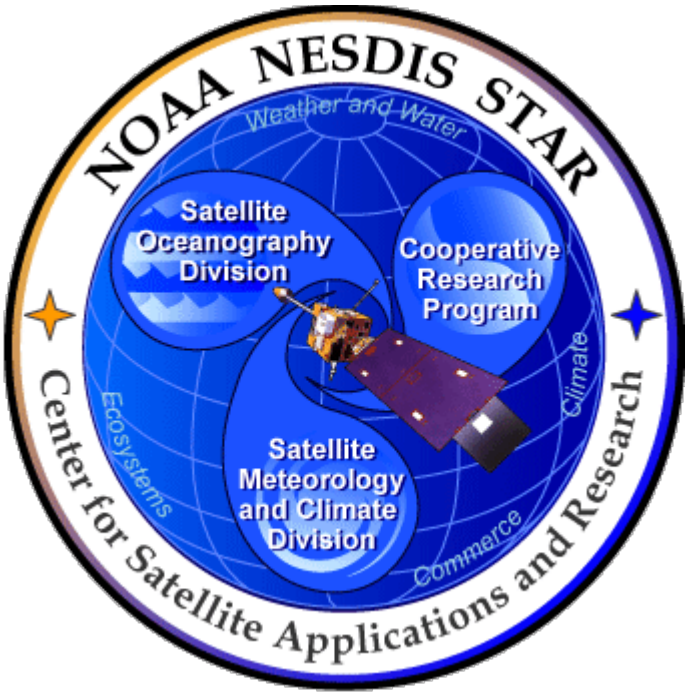

NOAA NESDIS
CENTER for SATELLITE APPLICATIONS and RESEARCH

GOES-R Advanced Baseline Imager (ABI) Algorithm Theoretical Basis Document For Land Surface Temperature

Yunyue Yu, NOAA/NESDIS/STAR
Peng Yu, ESSIC/CISESS, UMD

Version 4.0
June 4, 2020

Algorithm Theoretical Basis Document for Land Surface Temperature
Version History SUMMARY

Version	Description	Revised Sections	Date
0.1	New ATBD Document according to NOAA /NESDIS/STAR Document Guideline		6/15/2008
0.2	ATBD Document according to NOAA /NESDIS/STAR Document Guideline		9/30/2008
1.0	ATBD Document 80% readiness		6/26/2009
1.1	Modification made reflecting the responses to AIT and IV&V reviewer's comments, and for including testing results from using MODIS data		9/25/2009
2.0	Revision for reflecting further developments since version 2.0, and modifications and improvement based on the responses to reviewers comments/suggestions on version 2.0 from the IV&V, ADEB, SE members. Detail quality control flags and metadata information are provided. More test and validation results are added as well.	Sections 1 to 5.	6/28/2010
3.0	1) Modifications corresponding to the responses to reviewers comments; 2) word error corrections; 3) revision of the quality flags and relevant tables; 4) reference update		7/10/2012
4.0	Major revision: 1) Transition from the baseline algorithm to the enterprise algorithm; 2) Inclusion of algorithm mitigation associated with the GOES-17 Loop Heat Pipe issue; 3) Update of the product input and output		5/20/2020

Authors of previous versions:

Yunyue Yu, NOAA/NESDIS/STAR
Dan Tarpley, Short & Associates, Inc.
Hui Xu, and Ming Chen, I and M System Group, Inc.

TABLE OF CONTENTS

LIST OF FIGURES

Page

LIST OF TABLES

Page

LIST OF ACRONYMS

ABI	Advanced Baseline Imager
ACM	ABI Cloud Mask
ADEB	Algorithm Development Executive Board
AIADDD	Algorithm Interface and Ancillary Data Description Document
AIT	Algorithm Integration Team
AMSR-E	Advanced Microwave Scanning Radiometer - Earth Observing System
AMSU	Advanced Microwave Sounding Unit
ATBD	Algorithm Theoretical Base Document
AVN	The Aviation Model
AVHRR	Advanced Very High Resolution Radiometer
AWG	Algorithm Working Group
CIMSS	Cooperative Institute for Meteorological Satellite Studies
CONUS	Continental United States
ECMWF	European Centre for Medium-range Weather Forecasts
EOS	Earth Observation Systems
FD	Full Disk
FSC	Fraction of Snow Cover
FTP	File Transfer Protocol
G	Goal
GFS	Global Forecast System
GOES	Geostationary Operational Environmental Satellite
GS-F&PS	Ground Segment Functional and Performance Specification
IMS	Interactive Multi-sensor snow and ice mapping System
IR	Infrared
IV&V	Independent Verification and Validation
KIT	Karlsruhe Institute of Technology
LSA-SAF	Land Surface Analysis - Satellite Applications Facility
LST	Land Surface Temperature
LZA	Local Zenith Angle
M	Mesoscale
MODIS	Moderate Resolution Imaging Spectroradiometer
MRD	Mission Requirement Document
MSG	Meteosat Second Generation
NCEP	National center for Environmental Prediction
NESDIS	National Environmental Satellite, Data, and Information Service
NOAA	National Oceanic and Atmospheric Administration
NPOESS	National Polar-orbiting Operational Environmental Satellite System
NPP	The NPOESS Preparatory Project
NSIDC	National Snow and Ice Data Center
PIR	Precise Infrared Radiometer
PORD	Performance Operational Requirements Document

PQI	Product Quality Information
QA	Quality Assurance
QC	Quality Control
QF	Quality Flag
RTM	Radiative Transfer Model
SatZen	Satellite Zenith Angle
SDR	Sensor Data Record
SE	System Engineering
SEVIRI	Spanning Enhanced Visible and Infrared Imager
SolZen	Solar Zenith Angle
SRF	Spectral Response Function
SSEC	Wisconsin Space Science and Engineering Center
SSMI	Special Sensor Microwave Imager
SST	Sea Surface Temperature
STAR	Center for Satellite Applications and Research
STD	Standard Deviation
SURFRAD	SURFace RADiation network
SW	Split Window
SWA	Software Architecture Document
T	Target
TIR	Thermal Infrared
TOA	Top Of Atmosphere
TPW	Total Precipitable Water
UMD	University of Maryland
USAF	United States Air Force
VAGL	Vender Allocated Ground Latency
VIIRS	Visible/Infrared Imager /Radiometer Suite
VVP	Verification and Validation Plan
WV	Water Vapor

ABSTRACT

This Algorithm Theoretical Basis Document (ATBD) describes in detail the procedures to develop and use a land surface temperature (LST) algorithm designed for the GOES-R Advanced Baseline Imager (ABI). It includes a description of the requirements and specifications of the LST products and some specific information about the ABI that is relevant to the derivation of the LST products. The core of the ATBD is a description of the science of the proposed ABI LST algorithm, as well as a review of satellite LST research, a selection of candidate algorithms, and a description of a large simulated GOES-R ABI data set used to derive algorithm coefficients and test the candidate algorithms. The simulated brightness temperatures are calculated using sensor spectral response functions (SRF) from the actual ABI instrument. A description of the algorithm implementation is provided and ancillary data sets as input for the LST calculation are listed.

An enterprise LST retrieval algorithm applicable to both GOES-R and JPSS missions was developed and evaluated. Compared to the baseline algorithm, it includes the emissivity difference between the two split-window bands and replaced the path correction term with a stratification of the algorithm by satellite view zenith angle to allow better flexibility. Algorithm regression coefficients were derived from the simulated data set and have been tested with the satellite data from both GOES-16 and GOES-17 and the corresponding in-situ LST measurement from SURFRAD network. The algorithm was expected to meet the mission requirement and outperform the baseline algorithm.

An alternative LST retrieval algorithm was developed in order to mitigate the overheating of the GOES-17 ABI sensor. The algorithm adopts a similar formula as the enterprise algorithm but uses bands 13 and 14 instead of the combination of bands 14 and 15 as in both the baseline algorithm and the enterprise algorithm. Evaluation of the retrieval with in-situ data indicated good performance. It is expected to improve both the data quality and availability of the GOES-17 LST during the “hot” period. The enterprise and mitigation algorithm package is scheduled to replace the current baseline algorithm in July 2020.

1 INTRODUCTION

The purpose, users, scope, related documents and revision history of this document are briefly described in this section. Section 2 gives an overview of the land surface temperature (LST) retrieval objectives and operations concept. Section 3 describes the enterprise algorithm and the mitigation algorithm, the input data requirements, and the theoretical background. Test data sets and algorithm evaluation results are presented in Section 4. Some practical considerations are described in Section 5, followed by the assumptions and limitations associated with the algorithm in Section 6. Finally, Section 7 lists the references cited.

1.1 Purpose of This Document

This Algorithm Theoretical Basis Document (ATBD) explains the physical and mathematical background for an algorithm to derive LST product as part of the requirements for the Advanced Baseline Imager (ABI). ABI is the primary visible and infrared instrument onboard the platform of the Geostationary Environmental Operational Satellite (GOES) R series (GOES-R) of NOAA meteorological satellites. This document provides an overview of the required input data, the physical and mathematical backgrounds of the described algorithm and its predicted performance, practical considerations, and assumptions and limitations.

1.2 Who Should Use This Document

The intended users of this document are those interested in understanding the physical bases of the LST algorithm and how to use the output of this algorithm for a particular application. This document also provides information useful to anyone maintaining or modifying the original algorithm.

1.3 Inside Each Section

This document covers the theoretical basis for the derivation of the LST product from ABI data. It is broken down into the following main sections:

- **System Overview**: provides objectives of the LST algorithm, relevant details of the ABI instrument, and a brief description of the product requirements.
- **Algorithm Description**: provides all the detailed description of the algorithm including its physical basis, its input and its output.
- **Test Datasets and Outputs**: provides detailed information of the evaluation of the enterprise algorithm and mitigation algorithm using actual GOES-R ABI data.
- **Assumptions and Limitations**: provides an overview of the current limitations of the algorithm and gives the plan for overcoming these limitations with further algorithm development.

1.4 Related Documents

This document may contain information from other GOES-R documents listed in the website provided by GOES-R algorithm working group (AWG):
https://www.goes-r.gov/resources/docs.html.

In particular, readers are directed to read the following documents for good understanding of this ATBD:

GOES-R Series Ground Segment Functional and Performance Specification
GOES-R Series Mission Requirements Document
GOES-R Land Surface Team Critical Design Review
GOES-R Algorithm Theoretical Base Document for ABI Cloud Mask

Other related references are listed in the Reference Section.

1.5 Revision History

Version 0.1 of this document was created by Dr. Yunyue Yu of NOAA/NESDIS, and its intent was to accompany the delivery of the version 0.5 algorithm to the GOES-R AWG Algorithm Integration Team (AIT)**.** The document was then revised following the document guideline provided by the GOES-R Algorithm Application Group (AWG) before the version 1.0 delivery. In 2009 spring and summer, version 1.0 of the document was prepared, which includes some new results conducted from the algorithm Critical Design Review (CDR) and the Test Readiness Review (TRR), as the algorithm 80% readiness document. For version 1.1 in September 2009, modification has been made reflecting the responses to AIT and IV&V reviewer's comments. It also includes testing results from using MODIS data. Version 2.0 was completed in July 2012, including responses to all the review comments from the AIT, the ADEB, and the Harris, along with some further development on the algorithm evaluation and testing, quality control flags and metadata definition. The current version, version 4.0, is prepared to document the most significant updates since the launch of GOES-R, including the development and evaluation of the enterprise algorithm for both GOES-16 and GOES-17, the mitigation algorithm for GOES-17 during the "hot" period, and the corresponding changes of the algorithm input and output.

2 OBSERVING SYSTEM OVERVIEW

This section describes objectives of the LST algorithm, details of the ABI instrument, and requirements of the product.

2.1 Products Generated

LST is one of the key variables in the weather and climate system controlling surface heat and water exchange at the land atmosphere interface. Satellite measured LST is mostly based on thermal infrared band observations, which theoretically gives the temperature at some nominal skin depth of the surface. In the GOES-R mission, LST is measured from its onboard ABI. Knowledge of LST gives critical information on temporal and spatial variations of the surface equilibrium state and is of fundamental importance to many aspects of geoscience. Remotely sensed LST can be assimilated into weather and climate models to optimize weather and climate predictions (Meng et al, 2009; Zheng et al, 2012; Trigo et al, 2015), be applied as input data for mesoscale atmospheric and land surface models to estimate sensible heat flux and latent heat flux, or be utilized to evaluate the model prediction performance. It has been widely used in commercial applications including the evaluation of water requirements for crops in summer and to estimate where and when damaging frost may occur in winter. LST can also provide warning signs for possible forest and grass fires, as well as an indicator of possible drought, just to name a few (Karnieli et al., 2010; Zhang et. al., 2014; Quintano et. al., 2015; Fang et. al, 2019). In 2016, World Meteorological Organization included LST as one of essential climate variables (ECV) in the Global Climate Observing System (GCOS, 2017).

In the GOES-R program, the LST product is generated in three scanning coverages: Contiguous United States (CONUS), Full Disk (FD), and Mesoscale (MESO), with a requirement of 2.5 K in accuracy and 2.3 K in precision. Detailed specifications of the LST product are defined in the GOES-R mission requirement document (MRD) and will be briefly described in the next section.

Accuracy of the satellite LST measurement is limited by the atmospheric correction, the complexity of surface emission characteristics, and the sensor performance. The algorithm performance varies significantly over area, season, view geometry, and atmospheric water vapor conditions (Yu et al, 2009b, 2012; Coll et al, 2005, 2010, 2012; Hook et al, 2007; Hulley and Hook, 2011, Guillevic et al, 2012; Wan et al, 2004, Wan, 2008, 2014; Li et al, 2013; Liu et al, 2015; Göttsche et al, 2016). A primary objective of the GOES-R LST development team is to provide a state-of-the-art LST algorithm that meets the GOES-R mission requirement. Retrievals of LST have been conducted for over forty years from a variety of polar-orbiting and geostationary satellites. To produce an LST climate data record from those programs, consistency among LST products from different satellite missions is of importance. The GOES-R LST algorithm should have a good historical heritage for consistency with other satellite products. These factors as well as the algorithm simplicity and robustness have been considered throughout the development phase of the algorithm.

2.2 Instrument Characteristics

The ABI is a mission critical payload on GOES-R, providing a majority of all the mission data products currently defined. Similar to its predecessor, the GOES imager, ABI has been used for a wide range of qualitative and quantitative weather, oceanographic, climate, and environmental applications. ABI offers more spectral bands, higher spatial resolution, and faster imaging rate than the GOES imager. Its spatial resolution is nominally 2 km for the infrared bands and 0.5 km for the 0.64 μm visible band. While the instrument allows a flexible scanning scenario, three basic modes, Modes 3, 4, and 6, have been tested and implemented since its operation. Mode 3, the previous default scan mode, scans the FD every 15 minutes, the CONUS every 5 minutes, and a selectable 1000 km ×1000 km area every 30 seconds; Mode 4 provides continuous FD scans every five minutes; Mode 6, the current default mode, scans the FD every 10 minutes, its scan schedule over CONUS and MESO is similar to that of Mode 3. As a comparison, the GOES imager takes approximately 25 minutes for a FD; GOES-R provides a fivefold increase in the coverage frequency (Schmit *et al.*, 2016).

ABI has 16 spectral bands; five are similar to the 0.6-, 4-, 11-, and 12-μm windows and the 6.5-μm water vapor band on the GOES-8/-9/-10/-11 imagers (Menzel and Purdom, 1994; Ellrod *et al.*, 1998) and one is similar to the 13.3 μm on the GOES-12/-13/-14/-15 imagers and the GOES-8/-15 sounders (Hillger and Gary, 2003; Schmit *et al.*, 2002). Additional bands on ABI are 0.47 μm for aerosol detection and visibility estimation; 0.865 μm for aerosol detection and estimation of vegetation index and health; 1.378 μm to detect very thin cirrus clouds; 1.6 μm for snow/cloud discrimination; 2.25 μm for aerosol and cloud particle size estimation, vegetation, cloud properties/screening, hot-spot detection, moisture determination, and snow detection; 7.0 and 7.34 μm for midtropospheric water vapor detection and tracking and upper-level sulfur dioxide (SO_2) detection; 8.5 μm for detection of volcanic dust clouds containing sulfuric acid aerosols and estimation of cloud phase; 9.6 μm for monitoring atmospheric total column ozone and upper-level dynamics (Steinbrecht *et al.*1998); and 10.35 μm for deriving low-level moisture and cloud particle size. Each of these bands is often used in conjunction with other bands in a multiple spectral approach for product generation. Figure 2.1 shows the spectral distribution of the ABI channels, compared to the GOES-12 imager channels, while channel specification of the ABI is given in Table 2.1. The advanced design of ABI will provide users with twice the spatial resolution, five times the scan rate, and more than three times the number of spectral channels compared to the GOES imager (Schmit *et al.*, 2016). These improvements allow meteorologists and climatologists to significantly improve the accuracy of their products, both in forecasting and nowcasting.

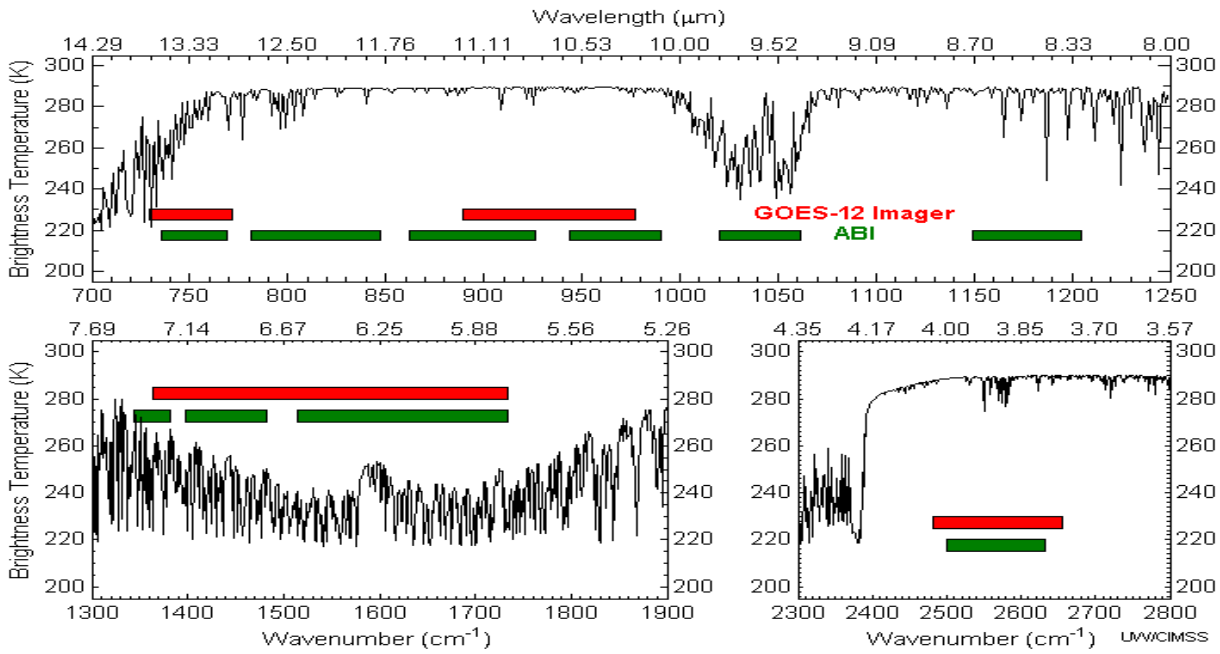

Figure 2.1. Spectral distribution of the ABI channels, compared to the current GOES (GOES-12) Imager channels.

Table 2.1. Spectral characters of Advanced Baseline Imager.

Channel Number	Wavelength (μm)	Bandwidth (μm)	NEDT/SNR	Upper Limit Of Dynamic Range	Spatial Resolution
1	0.47	0.45 – 0.49	300:1[1]	652 W/m^2/sr/μm	1 km
2	0.64	0.59 – 0.69	300:1[1]	515 W/m^2/sr/μm	0.5 km
3	0.86	0.8455 – 0.8845	300:1[1]	305 W/m^2/sr/μm	1 km
4	1.38	1.3705 – 1.3855	300:1[1]	114 W/m^2/sr/μm	2 km
5	1.61	1.58 – 1.64	300:1[1]	77 W/m^2/sr/μm	1 km
6	2.26	2.225 – 2.275	300:1[1]	24 W/m^2/sr/μm	2 km
7	3.9	3.8 – 4.0	0.1K[2]	400K	2 km
8	6.15	5.77 – 6.60	0.1K[2]	300K	2 km
9	7.0	6.75 – 7.15	0.1K[2]	300K	2 km
10	7.4	7.24 – 7.44	0.1K[2]	320K	2 km
11	8.5	8.30 – 8.70	0.1K[2]	330K	2 km
12	9.7	9.42 – 9.80	0.1K[2]	300K	2 km
13	10.35	10.10 – 10.60	0.1K[2]	330K	2 km
14	11.2	10.80 – 11.60	0.1K[2]	330K	2 km
15	12.3	11.80 – 12.80	0.1K[2]	330K	2 km
16	13.3	13.0 – 13.6	0.3K[2]	305K	2 km

[1]100% albedo, [2]300K scene. Shaded channels are used for LST retrieval.

The land surface temperature will be produced for each cloud free land pixel observed by the ABI sensor. The LST retrieval will primarily rely on channels 14 and 15 of the ABI data using split window technique.

2.3 Mission Requirement

The LST requirements (Table 2.2) were originally defined in the mission requirement document (MRD), and further specified and updated in the Ground Segment Functional and Performance Specification (GS-F&PS). In this document we further specify that the LST is the instantaneous temperature of the earth "skin" as viewed from the satellite position, given the particular sun-view geometry.

Table 2.2. GOES-R mission requirements for land surface temperature.

Observational Requirement	LEVEL[1]	Geographic Coverage[2]	Horiz. Res.	Mapping Accuracy	Msmnt. Range (K)	Msmnt. Accuracy[3] (K)	Msmnt. Precision (K)	Refresh Rate	VAGL[4]	Long-term Stability	Extent Qualifier[5]
LST (Skin): CONUS	T	C	2 km	1 km	213 – 330	2.5	2.3	60 min	3236 sec	TBD	LZA <70
LST (Skin): Hemispheric	T	FD	10 km	5 km	213 – 330	2.5	2.3	60 min	806 sec	TBD	LZA <70
LST (Skin): Mesoscale	T	M	2 km	1 km	213 – 330	2.5	2.3	60 min	159 sec	TBD	LZA <70

[1] T=target, G=goal
[2] C=CONUS, FD=full disk, H=hemisphere, M=mesoscale
[3]The measurement accuracy 2.5K is conditional with 1) known emissivity, 2) known atmospheric correction and 3) 80% channel correction; 5 K otherwise.
[4] VAGL=Vender Allocated Ground Latency.
[5] LZA=local zenith angle.

3 ALGORITHM DESCRIPTION

A complete description of the algorithm at the current level of maturity (which will improve with each revision) is given in this section.

3.1 Algorithm Overview

The LST is one of the baseline products in the GOES-R ABI processing system and is on the priority development list of the GOES-R algorithm working group (AWG). Its retrieval algorithm is developed by the GOES-R AWG land team within the land module processing subsystem (Figure 3.1).

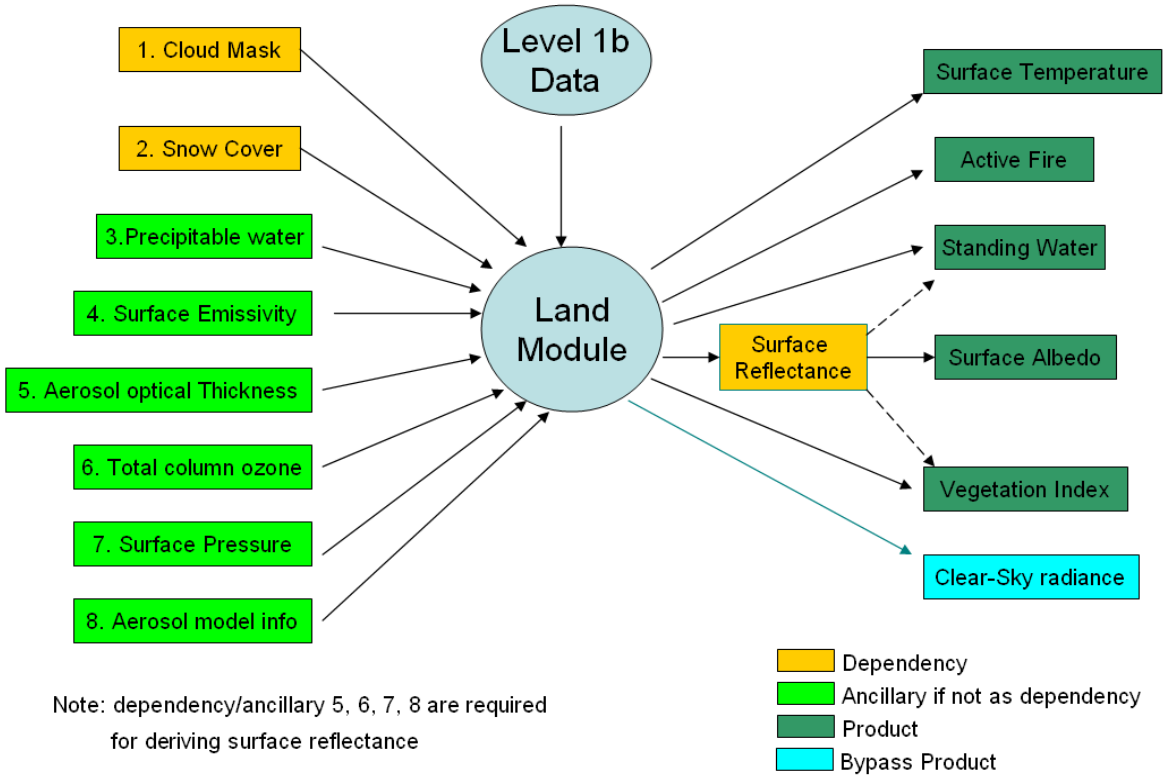

Figure 3.1. Products and dependencies of the land algorithm module.

The LST retrieval algorithm for GOES-R mission currently in operation is the so-called baseline algorithm, which was developed by Yu *et. al.* (2008, 2009a). The algorithm was selected among nine candidate algorithms based on a comprehensive analysis and testing. Due to its performance, robustness, and simplicity, the algorithm (Eq 3.1) adapted from Ulivieri & Cannizzaro (1985) was selected and became operational baseline algorithm.

$$T_s = C + A_1 T_{11} + A_2 (T_{11} - T_{12}) + A_3 \varepsilon + D(T_{11} - T_{12})(\sec\theta - 1) \qquad (3.1)$$

where T_{11} and T_{12} represent the top-of-atmosphere brightness temperatures at ~11 μm and ~12 μm, respectively, $\varepsilon = 0.5 * (\varepsilon_{11} + \varepsilon_{12})$ is the average of the spectral emissivity of the land surface at ~11 μm and ~12 μm, θ is the satellite view zenith angle, and $C,\ A_1,\ A_2,\ A_3,\ D$ are the

algorithm coefficients, stratified by day/night and dry/wet atmospheric conditions. More details about the baseline algorithm can be found in Appendix A and Yu *et. al.* (2009a).

Since the launch of GOES-16 satellite, the baseline algorithm has been in operation for three years. With this algorithm, the GOES-16 LST declared Provisional maturity in March 2018, and the GOES-17 LST during "cool" period declared Provisional maturity in June 2019.

There are two LST products from satellite missions operated by NOAA, the GOES-R mission and the JPSS mission. The algorithms used in these two products are different. Major differences lie in the input data to characterize the surface emission variability. The baseline algorithm for GOES-R LST uses the surface emissivity for this purpose, while the JPSS IDPS LST algorithm is based on surface types. Though both algorithms have their advantages, major drawbacks exist. In the baseline algorithm, the emissivity difference between the split-window channels is excluded and the atmospheric path length term is not able to fully represent the effect due to path with different atmospheric conditions. For the IDPS algorithm, the surface type cannot fully characterize the variability of the surface emission, especially the within-type variability. Therefore an enterprise retrieval algorithm applicable to both sensors have been developed and tested. This allows better consistency between the two products. In the meantime, efforts for both missions can be leveraged with each other.

3.2 Processing Outline

The processing outline of the LST is summarized in Figure 3.2. The LST retrieval starts from the module initialization and definition of parameters, including the FPM temperature threshold value, based on which the branch of either enterprise or mitigation algorithm is activated. For each pixel within the same satellite scene, the same algorithm is used. The LST configuration parameters and satellite navigation information are then loaded followed by major retrieval inputs, including the sensor data, emissivity, retrieval LUT, land/sea mask, cloud mask, snow/ice mask, ABI and/or NWP (numerical weather predictions) TPW (total precipitable water), and AOD (aerosol optical depth) . The quality flags are determined for all pixels while LST is retrieved for each cloud free land pixel. Finally, the calculated LST values and their associated quality control flags, which were generated in each of the above steps, are combined and output to files for user access.

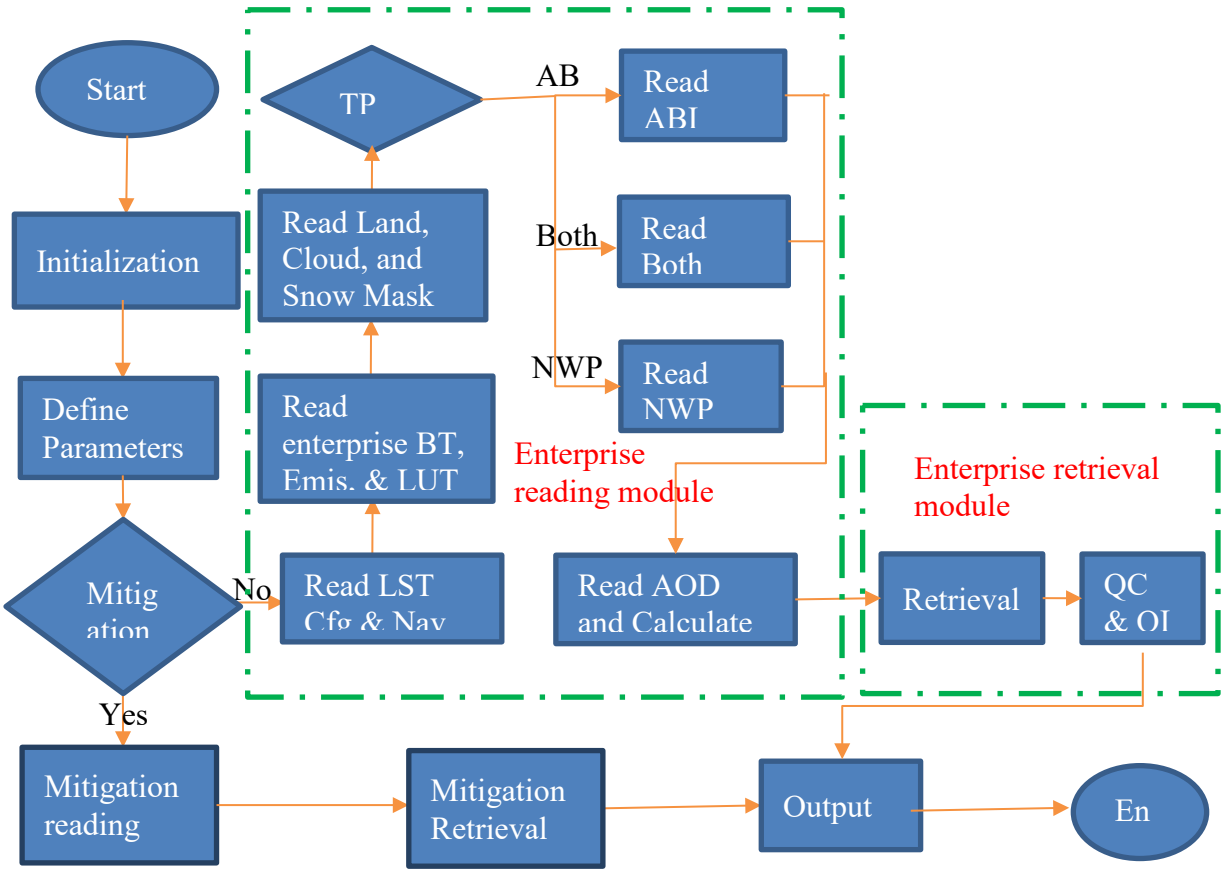

Figure 3.2. High level flowchart of the LST production for illustrating the main processing steps.

3.3 Algorithm Input

This section describes the input needed to process the LST product. To derive the LST for each pixel, ancillary datasets are required as well as the upstream ABI data.

3.3.1 Primary Sensor Data

The list below contains the primary sensor data used by the LST retrieval. By primary sensor data, we mean information that is derived solely from the ABI observations and geolocation information, or the level 1b data. Table 3.1 lists those input sensor data and their descriptions. All input data will be used at the high resolution level and the aggregation method for generating the hemispheric scale LST product at 10 km resolution will only be applied to the output product.

Table 3.1. Input list of primary sensor data.

Name	Type	Description	Dimension	Unit
FPM temperature	Input	Focal plane module temperature	scalor	Degree K
Ch13 brightness temperature	input	Calibrated ABI level 1b brightness temperatures at channel 13	grid (xsize, ysize)	Degree K
Ch14 brightness temperature	input	Calibrated ABI level 1b brightness temperatures at channel 14	grid (xsize, ysize)	Degree K
Ch15 brightness temperature	input	Calibrated ABI level 1b brightness temperatures at channel 15	grid (xsize, ysize)	Degree K
Latitude	input	Pixel latitude	grid (xsize, ysize)	Degree
Longitude	input	Pixel longitude	grid (xsize, ysize)	Degree
Solar zenith	input	ABI solar zenith angles	grid (xsize, ysize)	Degree
View zenith	input	ABI view zenith angle	grid (xsize, ysize)	Degree
QC flags	input	ABI quality control flags with level 1b data	grid (xsize, ysize)	Unitless

- **FPM temperature**

The temperature of the FPM used to determine which algorithm to be activated for LST retrieval. Its unit is degree of Kelvin.

- **ABI channel input**

The GOES-R ABI channel brightness temperatures at 10.35 μm, 11.2 μm and 12.3 μm are used for LST calculation. The pixel resolution should be 2 km and the brightness temperature should be in unit of Kelvin.

- **Geolocation data**

Latitude and longitude information for each pixel is needed for mapping the sensor data to ancillary data applied. They should be part of the Level 1 ABI data and the unit used for calculation should be in degrees.

- **Viewing geometry information**

Solar zenith angle is needed to determine day and night condition. The satellite view zenith angle is used for atmospheric path correction, which is part of the algorithm application. Details of their usage for LST derivation will be described in later sections.

- **QC flags in the level 1 ABI data**

Any inherent QC flags in the level 1 ABI data will be read and applied before generating LST using the selected algorithm. Any missing/bad pixels will be skipped.

3.3.2 Derived Sensor Data

GOES-R ABI derived sensor data sets (or the ABI related ancillary dataset quoted earlier) used by the LST retrieval are listed in Table 3.2 and described in this section.

Table 3.2. Input list of derived sensor data.

Name	Type	Description	Dimension	Unit
Cloud mask	input	ABI level 1cloud mask data	grid (xsize, ysize)	unitless
Snow/Ice mask	input	ABI level 2 Snow/Ice mask data	grid (xsize, ysize)	0-1.0 fraction of snow cover
Total Precipitable Water	input	ABI baseline TPW	grid (xsize, ysize)	mm
Aerosol Optical Depth	input	ABI level 2 aerosol optical depth	grid (xsize, ysize)	unitless
Land Surface Emissivity	input	ABI level 2 land surface emissivity	grid (xsize, ysize)	unitless

- **Cloud mask**

The ABI cloud mask (ACM) algorithm generates the option 1 product of a binary clear-sky mask, as well as a 4-level cloud mask which indicates four cloudiness conditions for each pixel: clear, probably clear, probably cloudy, and cloudy. Information about thin cirrus and active fire used to determine the LST quality flag is included in this product.

- **Total precipitable water**

The GOES-R AWG sounding team has developed the algorithm to generate the TPW as one of the baseline products, covering CONUS, full disk and mesoscale, with a horizontal resolution of 10 km and accuracy at 1 mm and precision at 3 mm. This product offers better quality, higher spatial and temporal resolutions than the current NCEP forecast data. The ABI TPW is the primary TPW input for the LST algorithm.

- **Aerosol optical depth**

The AOD is used as one of the input to determine the LST quality flag.

- **Surface emissivity**

Land surface emissivity is an option-2 ABI product retrieved using time continuity. This product would be the preferred input to LST algorithm because of the higher spatial, temporal resolutions and better quality in comparison to the monthly mean emissivity retrieval. Alternatively, MODIS monthly emissivity dataset is applicable for the purpose.

- **Snow/Ice mask**

Currently, snow cover is an ABI level-2 product measured as a fraction of snow cover (FSC) with a refresh rate of 60 minutes and ice cover is another ABI level-2 product with a refresh rate of every 180 minutes. The snow/ice mask can be derived from these ABI level-2 products.

In case the ABI snow/ice mask is not available at the GOES-R operational, the Interactive multi-sensor snow and ice Mapping System (IMS) will be used for the snow/ice mask.

3.3.3 Ancillary Data

The following table lists and briefly describes the ancillary data required to run the LST. By ancillary data, we mean data that requires information not included in the ABI observations or geolocation data.

Table 3.3 Input of ancillary data.

Name	Type	Description	Dimension
Land/sea mask	input	A land-ocean mask	grid (xsize, ysize)
Water vapor*	input	NCEP water vapor 6-hour forecast data	0.25 deg resolution
Emissivity*	input	MODIS monthly emissivity	0.05 deg resolution
IMS snow/ice mask*	input	Interactive multi-sensor snow and ice Mapping System	0.05 deg resolution

* Alternative input data in case the corresponding ABI product is not available at the GOES-R operation.

- **Land/Sea mask**

The 1 km resolution land/sea mask will be used for GOES-R ABI products. It is created by SSEC/CIMSS based on NASA MODIS collection 5. Several categories are available in the land/sea mask, including shallow, moderate and deep oceans, land, shoreline, shallow, ephemeral, and deep inland water. LST will be calculated for all land and inland water pixels.

- **Water vapor**

The water vapor information is extracted from the NCEP analysis and model forecast data. The Aviation model (AVN) provides global forecast every six hours and files in grib format can be downloaded through FTP. Currently we are using the 1° global coverage file, which may be replaced by higher resolution coverage at 0.25° in the future. An index file is available to point each ABI pixel to the corresponding TPW grid in the grib file.

- **Emissivity**

The Global Infrared Land Surface Emissivity is downloaded from the UW-Madison Baseline Fit Emissivity Database (http://cimss.ssec.wisc.edu/iremis/). This global database of infrared land surface emissivity is derived using input from the Moderate Resolution Imaging Spectroradiometer (MODIS) operational land surface emissivity product (MOD11). The baseline fit method (Seemann et al., 2007), based on a conceptual model developed from laboratory measurements of surface emissivity, is applied to fill in the spectral gaps between the six emissivity wavelengths available in MOD11. Emissivity in the baseline fit database is available globally at ten wavelengths (3.6, 4.3, 5.0, 5.8, 7.6, 8.3, 9.3, 10.8, 12.1, and 14.3 microns) with 0.05 degree spatial resolution. Corresponding emissivity values will be extracted and mapped into the ABI full disk area. They can then be applied to the LST algorithm to generate LST products.

It is worth pointing out that ABI emissivity data, which is the option 2 ABI product, should be used instead of the MODIS emissivity once it is ready.

- **Snow/Ice mask**

The IMS snow and ice product is available daily for northern hemisphere. It incorporates a wide variety of satellite imagery (AVHRR, GOES, SSMI, etc.) as well as derived mapped products (USAF Snow/Ice Analysis, AMSU, AMSR-E, NCEP models, etc.) and surface observations. The product is presently used as an operational input into several NWS computer weather prediction models as well as several other governmental agencies. Currently it is available at about 4 km (6144x6144) grid from NSIDC with a slight delay. Near real-time gridded data is available in ASCII format by request (http://www.natice.noaa.gov/ims/).

Details on the derivation of ancillary data can be referred to in the relevant AIT document "Algorithm Interface and Ancillary Data Description Document (AIADDD)". It is worth noting that LST is generated for snow/ice pixels but indicated with QC flags. Therefore the requirement for snow/ice mask is limited for the QC flag control. It is also worth noting that current ABI snow/ice product is quantitative out to 55 degree of LZA and qualitative beyond that, while the LST is required to be out to70 degree. A product quality information (PQI) flag is defined to indicate the LST is derived within 55° LZA, or alternative snow/ice mask will be used.

3.3.4 Algorithm Coefficients and Control values

In addition to the sensor data and the ancillary data, algorithm coefficients and some criterion values for algorithm selection and for quality control flags will be ingested as the input data.

3.4 Theoretical Description

Theoretical details of the research are provided in this section.

3.4.1 Physics of the Problem

In clear sky condition, the top of atmosphere (TOA) radiance ($I(\nu)$), which will reach to the satellite sensor, can be described by

$$I(\lambda) = I_s(\lambda) + I_{atm}(\lambda)^{\uparrow} + I_{atm}(\lambda)^{\downarrow} \qquad (3.2)$$

where $I_s(\lambda)$, $I_{atm}(\lambda)^{\uparrow}$ and $I_{atm}(\lambda)^{\downarrow}$ represent the radiance contributions from surface emission, atmospheric upwelling, and reflected downwelling radiance, respectively; λ is wave length of the sensing channel. The radiance components and their relationship are illustrated in Figure 3.3

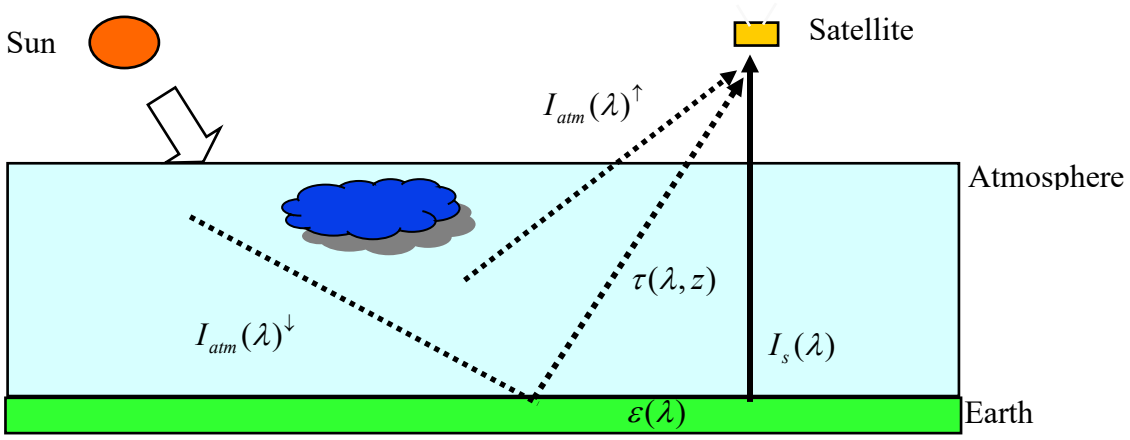

Figure 3.3. Radiation components reached to satellite sensor.

Satellite LST retrievals are usually performed in infrared (IR) bands where the surface emission reaches its maximum, yet atmospheric absorption is significantly small. In IR bands, each of the components in Eq (3.2) can be expressed mathematically by,

$$I_s(\lambda) = \varepsilon(\lambda)\tau_0(\lambda)B(\lambda, T_s)$$

$$I_{atm}(\lambda)^{\uparrow} = \int_z^0 B(\lambda,\ T_p(z))\frac{\partial\tau(\lambda,z)}{\partial z}dz \qquad (3.3)$$

$$I_{atm}(\lambda)^{\downarrow} = (1-\varepsilon(\lambda))\tau_0(\lambda)\int_0^z B(\lambda, T_p(z))\frac{\partial\tau(\lambda,z)}{\partial z}dz$$

where ε is the surface emissivity, τ is the atmospheric transmittance (τ_0 is the atmospheric transmittance from surface to top of atmosphere), z is the height from surface, T_s is the surface temperature, $T_p(z)$ is the atmospheric temperature at height z, and $B(\lambda, T_s)$ is the spectral radiance emitted by a blackbody at temperature T_s and wavelength λ, which can be calculated with the Planck function (Eq. 3.4).

$$B_\lambda(T_s) = \frac{c_1}{\lambda^5\left(\exp\left(\frac{c_2}{\lambda T}\right)-1\right)} \qquad (3.4)$$

where c_1 and c_2 are two constants ($c_1 = 1.191\times10^8 W\cdot\mu m^4\cdot sr^{-1}\cdot m^{-2}$, and $c_2 = 1.439\times10^4\mu m\cdot K$)

Eq. (3.2) and (3.3) are the so-called radiative transfer equations. All these magnitudes depend on the observation angle. From Equation (3.2), the earth surface emitted radiance $I_s(\lambda)$ is a function of temperature and emissivity and gets attenuated along the atmospheric path to the sensor. The purpose of the LST algorithm is to retrieve the land surface temperature T_s from the radiance

$I_s(\lambda)$ measured at the satellite sensor. In this problem, the surface temperature is physically coupled with two other factors: the surface emissivity and the atmospheric absorptions. Developing an LST algorithm means to find a solution to decouple the emissivity and the atmospheric absorption effects from the satellite received radiance.

3.4.2 Mathematical Description of the LST Algorithm

An analytic solution to equation (3.2) is not practical, because the integration of the terms requires good knowledge of the atmospheric profiles which is usually unavailable in real time. In addition, the land surface emissivity is coupled with the surface emission and reflection terms in the equation, so the number of unknowns is always larger than the number of equations, even though information from multiple channels is available. In the past thirty-five years, many approaches to the solution have been suggested (e.g., McMillin, 1975, Walton *et al.*, 1998), and widely used to produce the LST product (e.g., Prata, 1993 and 1994; Caselles *et al*., 1997; Wan, 1999).

3.4.2.1 The Candidate Algorithms

Over the past several decades, many algorithms have been proposed to treat the characteristics of various sensors onboard different satellites with different assumptions and approximations for the radiative transfer equation and the LSEs. These algorithms can be roughly grouped into three categories: single-channel methods, multi-channel methods, and multi-angle methods, provided that the LSEs are known a priori. If the LSEs are not known, the algorithms can be categorized into three types: stepwise retrieval method, simultaneous retrieval of LSEs and LST with known atmospheric information, and simultaneous retrieval (Li et al., 2013). The most widely used approach is the split window (SW) technique, in which the atmospheric effects are compensated using two or more adjacent TIR channels (typically at 10-12.5μm). The SW approach was first proposed by McMillin (1975) and has been successfully applied to retrieve sea surface temperature (SST). This method is simplistic and computationally efficient and does not require accurate atmospheric profiles. Encouraged by the success of the SW method in SST retrieval from the satellite measurements, many SW approaches have been proposed for LST retrieval (Atitar and Sobrino, 2008; Prata 1994; Price, 1984; Wan & Dozier, 1996, Sun et al., 2004) and widely used for producing the operational LST products (e.g., Wan, 1999; Caselles et al., 1997; Yu et al., 2009a; Sun et al., 2004; Hulley et al., 2016; Baker, 2013; Trigo et al., 2009; Liu et al., 2019). However, its application to LST retrieval is challenging due to the following reasons: first, compared to water surface, thermal IR (TIR) emissivity of most land surface types varies considerably from unity, leading to significant errors in the linearization of the radiative transfer equation which forms the basis for the SW technique (McMillin and Crosby, 1984). The remote sensing community has been working to obtain high quality global land surface emissivity data (e.g., Borbas et al., 2008; Seemann et al., 2008; Hulley & Hook, 2009; Hulley et al., 2015; Wang et al., 2019); second, topographical and vegetation structural variability is complicated and satellite sensed brightness temperatures over a given target can differ significantly from pixel to pixel; moreover, spatial heterogeneity is more significant over land than over ocean, and a retrieved LST represents a complex integration of the observed signal within a pixel; finally, the spatial and temporal variation of atmosphere over land is almost always greater than that over oceans.

To determine a GOES-R enterprise LST algorithm, we tried to simplify the above complexities by assuming that our prescribed surface emissivity values were sufficiently accurate and the angular and spatial variations described above were negligible. Note the GOES-R mission requirement document (MRD) and the GS-F&PS require use of emissivity values determined *a priori* (GOES-R Mission Requirement Document, 2007). Therefore, for the purposes of this document, we focused primarily on the atmospheric absorption correction issue. The SW technique is therefore a good choice since it is simple and robust for operational use, yet is sufficiently accurate to meet the mission's requirement.

We studied various SW LST algorithms from the literature (Price, 1984; Ulivieri and Cannizaro, 1985; Becker and Li, 1990; Prata and Platt, 1991; Vidal, 1991; Ulivieri *et al*., 1994; Sobrino *et al*., 1993, 1994; Wan and Dozier, 1996; Caselles *et al*., 1997; Coll *et al*., 1997; Yu *et al.*, 2008; Liu *el al*, 2019). We used eleven candidate algorithms including nine from the literature. (Table 3.4).

Table 3.4. Candidate split window LST algorithms.

No	Formula[#]	Reference
1	$T_s = C + \left(A_1 + A_2\frac{1-\varepsilon}{\varepsilon} + A_3\frac{\Delta\varepsilon}{\varepsilon}\right)(T_{11}+T_{12}) + \left(A_4 + A_5\frac{1-\varepsilon}{\varepsilon} + A_6\frac{\Delta\varepsilon}{\varepsilon}\right)(T_{11}-T_{12})$	Wan & Dozier (1996); Becker & Li (1990).
2	$T_s = C + A_1\frac{T_{11}}{\varepsilon} + A_2\frac{T_{12}}{\varepsilon} + A_3\frac{1-\varepsilon}{\varepsilon}$	Prata & Platt (1991); modified by Caselles *et al.* (1997).
3	$T_s = C + A_1T_{11} + A_2(T_{11}-T_{12}) + A_3(1-\varepsilon_{11}) + A_4\Delta\varepsilon$	Coll & Valor (1997).
4	$T_s = C + A_1T_{11} + A_2(T_{11}-T_{12}) + A_3\frac{1-\varepsilon}{\varepsilon} + A_4\frac{\Delta\varepsilon}{\varepsilon^2}$	Vidal (1991).
5	$T_s = C + A_1T_{11} + A_2(T_{11}-T_{12}) + A_3(T_{11}-T_{12})\varepsilon_{11} + A_4T_{12}\Delta\varepsilon$	Price (1984).
6	$T_s = C + A_1T_{11} + A_2(T_{11}-T_{12}) + A_3\varepsilon$	Ulivieri & Cannizzaro (1985).
7	$T_s = C + A_1T_{11} + A_2(T_{11}-T_{12}) + A_3\varepsilon + A_4\frac{\Delta\varepsilon}{\varepsilon}$	Sobrino *et al.* (1994).
8	$T_s = C + A_1T_{11} + A_2(T_{11}-T_{12}) + A_3(1-\varepsilon) + A_4\Delta\varepsilon$	Ulivieri *et al*. (1992).
9	$T_s = C + A_1T_{11} + A_2(T_{11}-T_{12}) + A_3(T_{11}-T_{12})^2 + A_4(1-\varepsilon_{11}) + A_5\Delta\varepsilon$	Sobrino *et al.* (1993).
10	$T_s = C + A_1T_{11} + A_2(T_{11}-T_{12}) + A_3\varepsilon + A_4\varepsilon(T_{11}-T_{12}) + A_5\Delta\varepsilon$	Additional algorithm #1

11	$T_s = C + A_1 T_{11} + A_2(T_{11} - T_{12}) + A_3\varepsilon + A_4\varepsilon(T_{11} - T_{12}) + A_5(T_{11} - T_{12})\Delta\varepsilon$	Additional algorithm #2
#Note: T_{11} and T_{12} represent the top-of-atmosphere brightness temperatures of ABI channels 14 and 15, respectively; $\varepsilon=(\varepsilon_{11}+\varepsilon_{12})/2$ and $\Delta\varepsilon=(\varepsilon_{11}-\varepsilon_{12})$, where ε_{11} and ε_{12} are the spectral emissivity values of the land surface at ABI channels 14 and 15, respectively; θ is the satellite view zenith angle. C, A_1, A_2, A_3, A_4, A_5, and A_6 are algorithm coefficients.		

As with most SW algorithms, our candidate algorithms explicitly use land surface emissivity values. This contrasts with algorithms such as Sun and Pinker (2004) and Sikorsky *et al.* (2002) where emissivity information is indirectly incorporated through the use of different coefficient sets determined for different land surface types. The latter approach must be tolerant to within-class emissivity variability which can be as significant as between-class variability. We prefer the algorithms of emissivity explicit since such algorithms allow easy incorporation of periodically updated land cover maps (e.g., annual maps from EOS/MODIS or seasonal from NPOESS/VIIRS), emissivity maps that accommodate within class variability (Yu *et al.*, 2005), maps that include directional variability (Yu *et al.*, 2006), or other related map improvements.

3.4.2.2 Algorithm Selection

The retrieval uncertainty of each candidate algorithm was analyzed with a comprehensive simulation dataset. The best performed algorithm was selected as the enterprise algorithm and its accuracy and precision were further tested with the satellite data and the in-situ LST measurements from the SURFace RADiation (SURFRAD) network.

The MODTRAN atmospheric radiative transfer model (Berk et al., 2000) has been widely used in satellite remote sensing studies for over three decades. We used the MODTRAN 5.2 in this study, which uses an improved molecular band model, termed the Spectrally Enhanced Resolution MODTRAN (SERTRAN). It has a much finer spectroscopy (0.1 cm^{-1}) than its predecessors (1 cm^{-1}), resulting in more accurate modeling of band absorption features in the longwave TIR window regions (Berk et al. 2005). The radiative transfer simulation procedure is illustrated in Figure 3.4.

The atmospheric profile database consists of 126 profiles generated from cloud-free radiosonde data available from the CrIS F98-Weather Products Test Bed Data Package (NOAA88, Rev. 1.0) and 354 profiles from Thermodynamic Initial Guess Retrieval (TIGR). TIGR data set, in its latest version, is a climatological library of 2311 representative atmospheric situations selected with statistical methods from 80,000 radiosonde reports (Chédin et al., 1985; Claud et al., 1991; Chevallier et al., 1998). Each situation is described, from the surface to the top of the atmosphere, by the values of the temperature, water vapor and ozone concentrations on a given pressure grid. TIGR profiles were checked by means of a cloud test in order to exclude impacts from cloud (Galve, 2008). The profiles represented a variety of atmospheric conditions, spanning a column water vapor range from 0.2 to 7.5 g/cm^2 and a surface air temperature range from 240 to 306 K (Figure 3.5) and spanned from 60º South to 70º North in latitude.

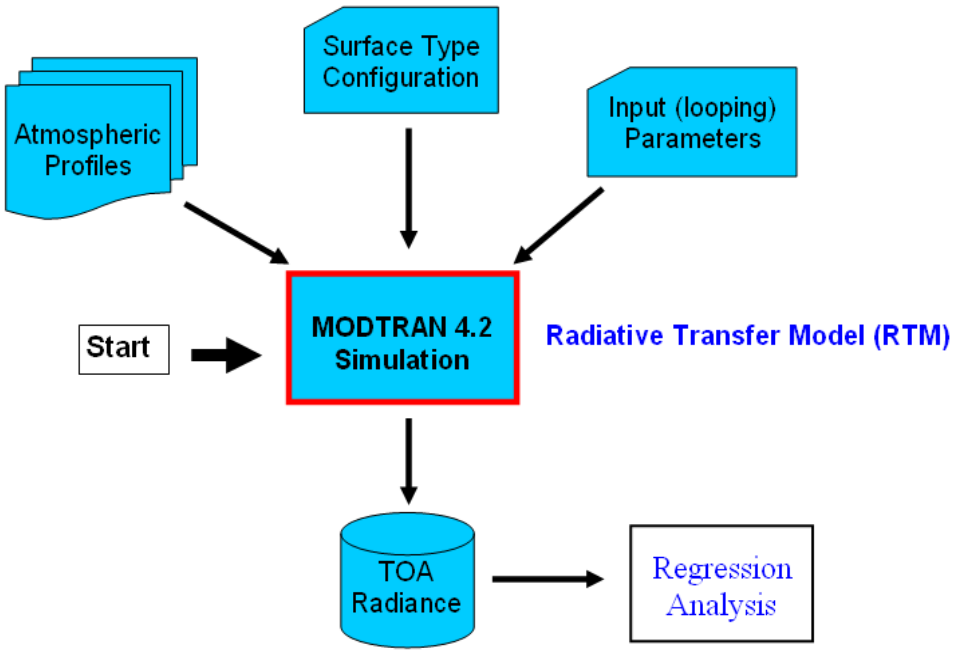

Figure 3.4. Radiative transfer simulation procedure.

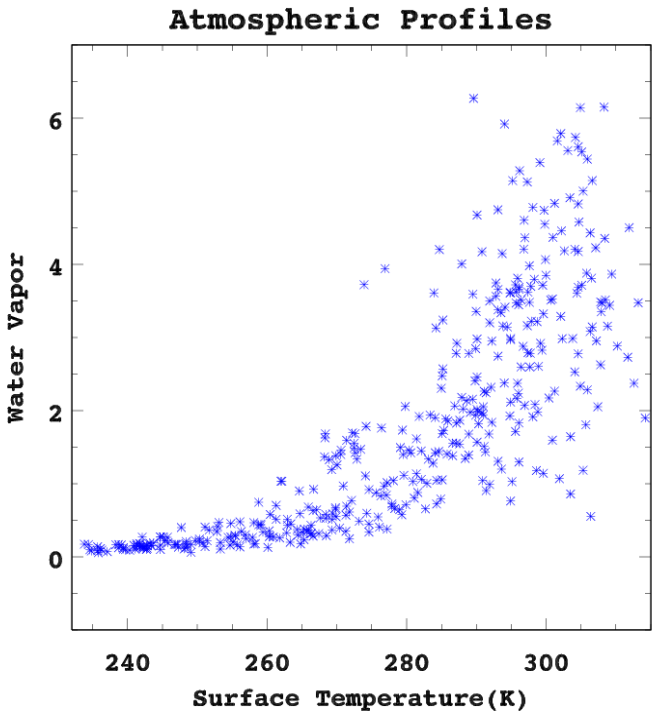

Figure 3.5. Distributions of total column water and surface air temperatures of the atmospheric profiles used in the simulation analyses.

To simulate a wide range of environmental conditions using a limited profiles set, we followed Yu *et al.* (2005) and varied the prescribed LST for each profile in a range as $Ts - 10 < LST < Ts + 10\ K$, where *Ts* is the land surface temperature of the profile, with a *1 K* increment. For each prescribed LST, we iterated the prescribed sensor view zenith angle from 0 to 70º with 10º increment and emissivity from 0.90 to 0.999 with a step of 0.00125.

Upon simulating the top-of-atmosphere radiances, we then conducted regression analyses for the algorithm development. The regression procedure is illustrated in Figure 3.6.

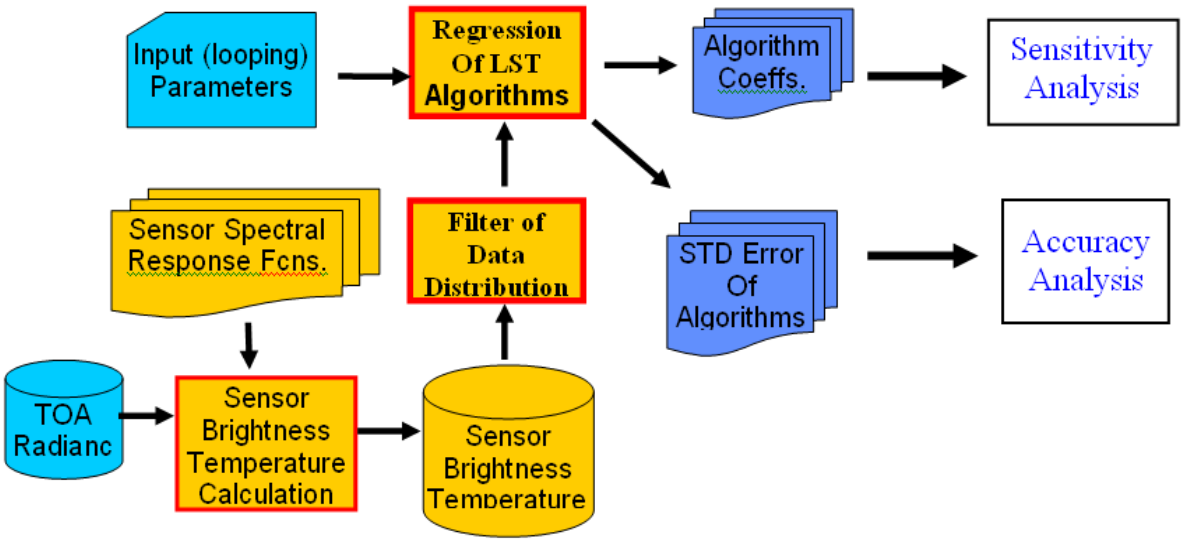

Figure 3.6. Procedure of the algorithm regression analyses.

We first determined the mean channel radiance by integrating over the ABI sensor spectral response function (SRF). The channel radiances were converted to corresponding brightness temperatures using the Planck function. This constructs a comprehensive brightness database for algorithm regression training.

Because water vapor is the most significant atmospheric absorber in the thermal bands, we stratified the simulation data according to the water vapor. The stratification acknowledges the capacity of warm atmospheres to hold more water vapor, as is shown in Figure 3.5, and the degradation of LST algorithm performance with increasing water vapor.

Due to significant differences in the discontinuity between LST and air temperature, during daytime and nighttime, many LST retrieval algorithms (or accompanying coefficient sets) were specified uniquely for daytime or nighttime use. We also performed regressions separately for the daytime and nighttime datasets. In addition, to better simulate real satellite data, we added Gaussian-distributed random noise to both the simulated brightness temperatures and the surface emissivity values. The standard deviations of the sensor Noise Equivalent Delta Temperature (NEΔT) and the surface emissivity noise are 0.1 K and 0.005 (unitless), respectively. The NEΔT value is the design requirement for ABI in channels 14 and 15; the assumed emissivity noise

standard deviation is 2.5 times the digitization error of the MODIS emissivity product, which is a candidate for the ABI LST derivation.

Before conducting regression analysis with the simulated data and candidate algorithms, we also considered the natural Gaussian-like distribution of land surface and surface air temperatures as noted in Justin *et al.* (NGST technical report, personal communication, 2006). That report used NCEP and ECMWF datasets for VIIRS LST algorithm analysis. We therefore applied a Gaussian function to filter the simulation data before running the algorithm regression process. Figure 3.7 shows the filtering results for the daytime dataset. A similar process was applied on the nighttime dataset.

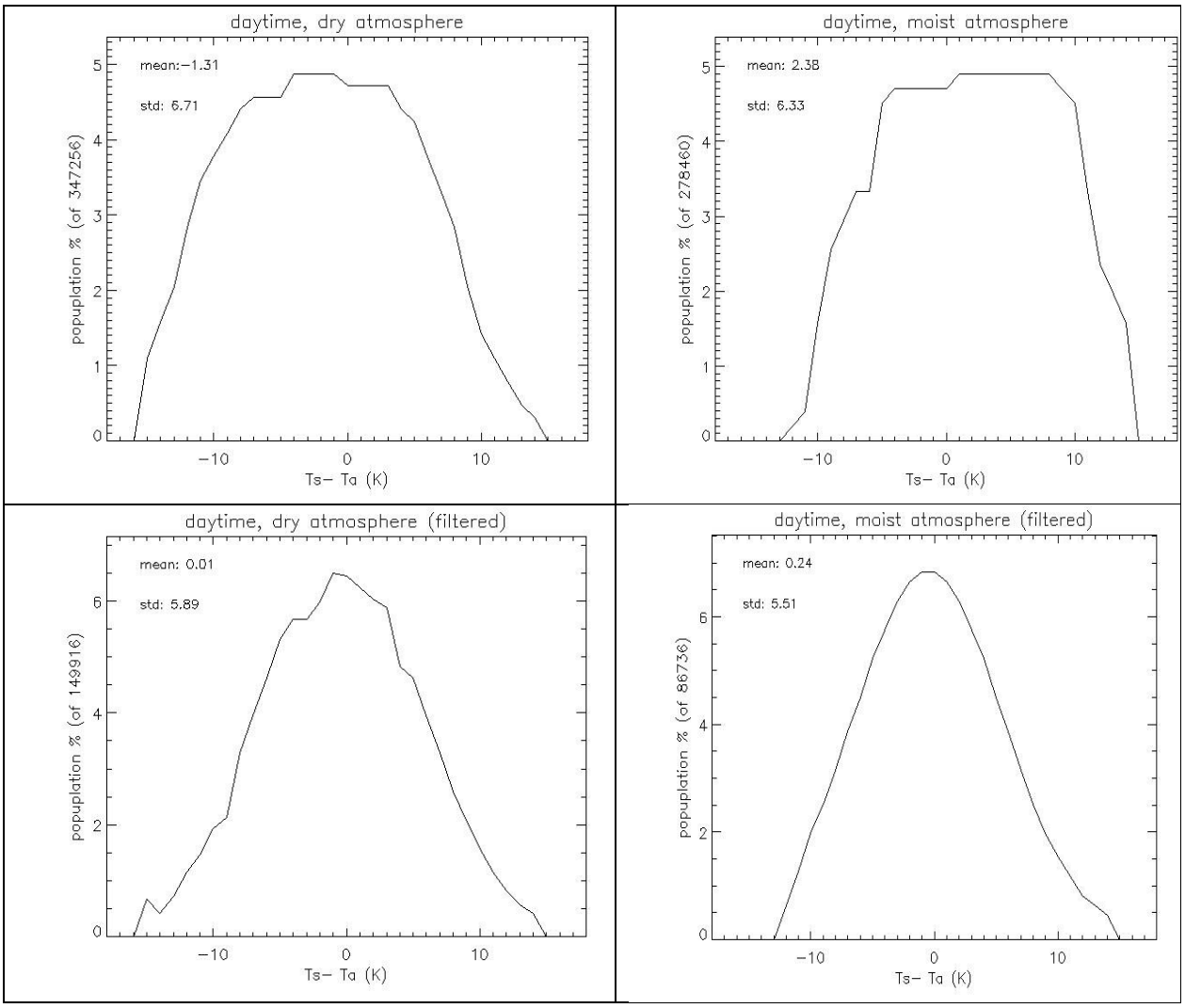

Figure 3.7. Daytime simulation data distribution in terms of the land surface and surface air temperature differences. The original simulation data (top panels) are pretty much evenly distributed in range of the temperature differences. The filtered data for both the dry (left) and moist (right) atmospheres are shown in the bottom panel.

3.4.2.3 The enterprise algorithm

For each of the eleven algorithms, we calculated the bias and standard deviation of the regressions. It was found that most algorithms were able to yield similar performance. This primarily indicates the accuracy limitation of the current SW technique.

Based on the algorithm performance, and its robustness and simplicity, additional algorithm # 1 (Eq. 3.5) was selected as the enterprise algorithm (Liu *et al.*, 2019).

$$T_s = C + A_1 T_{11} + A_2 (T_{11} - T_{12}) + A_3 \varepsilon + A_4 \varepsilon (T_{11} - T_{12}) + A_5 \Delta\varepsilon \qquad (3.5)$$

where definitions of T_{11}, T_{12}, and ε are the same as those in Eq. 3.1, $\Delta\varepsilon = (\varepsilon_{11} - \varepsilon_{12})$ is the difference of the spectral emissivity of the land surface at ~11 μm and ~12 μm, $C, A_1, A_2, A_3, A_4, A_5$ are the algorithm coefficients, stratified by day/night, atmospheric conditions, and satellite view zenith angles.

Compared to the baseline algorithm, there exist two major differences: 1) the emissivity difference between the two window channels is explicitly included in the retrieval formula; 2) the atmospheric path length term is replaced with the stratification by satellite zenith angle. It should be noted that all results assume perfect cloud detection. That is, all these results are for truly cloud clear pixels. Residual cloud effects in pixels detected as clear will add significant noise to the LST retrievals

3.4.2.4 The mitigation algorithm

During post-launch testing of the GOES-17 ABI instrument, an issue with the instrument's cooling system was discovered. The loop heat pipe (LHP) subsystem, which transfers heat from the ABI electronics to the radiator, is not operating at its designed capacity. The consequence of this is that the ABI detectors cannot be maintained at their intended temperatures under certain orbital conditions. Inadequate cooling of the infrared channels leads to partial loss of imagery during some of the overnight hours before and after the vernal and autumnal equinoxes.

Infrared signals with long wavelengths can be swamped by infrared light emitted by warm parts of the imager, degrading the signal. Cooling the detectors reduces this thermal "noise" in observations. During some nighttime hours during certain parts of the year (before and after the vernal and autumnal equinoxes) (Figure 3.8), the sun heats up seven of the ABI detectors faster than they can be cooled. The detectors become warmer than they're designed to operate, and they begin to radiate at temperatures closer to the wavelengths they're attempting to detect from the Earth. Eventually, local emissions and dark current noise overwhelm the signal from the Earth, and the channels saturate, meaning a useful signal is not available.

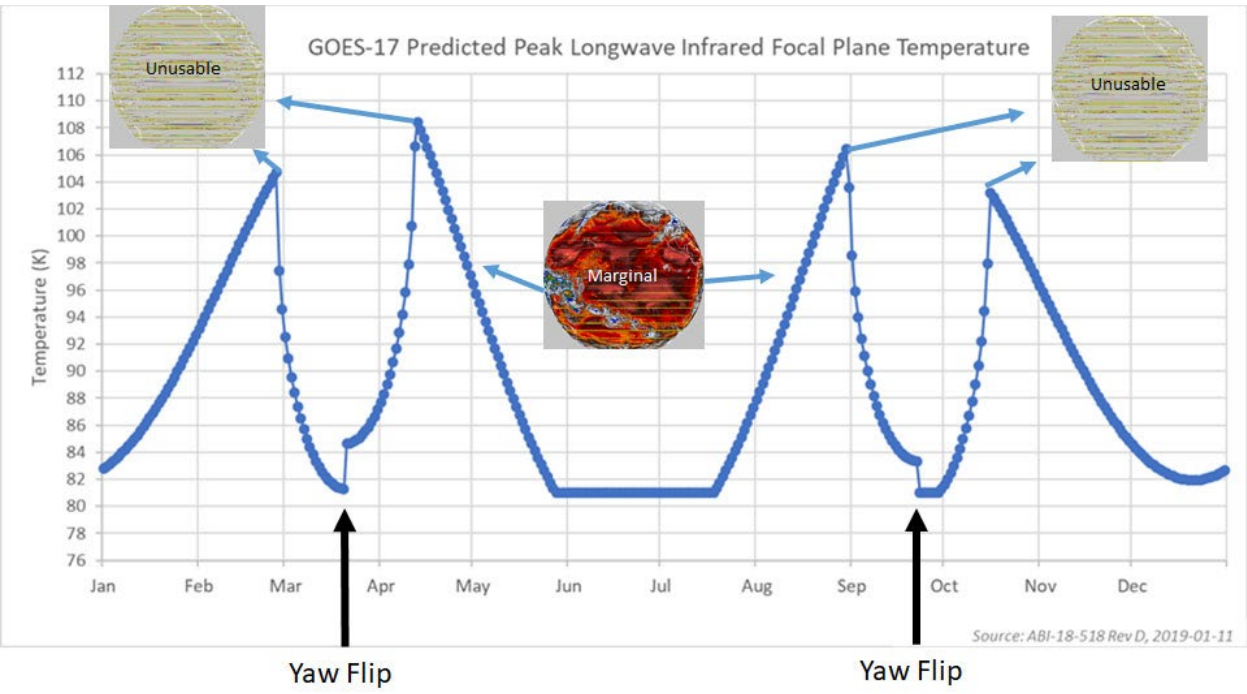

Figure 3.8. The 2019 prediction for peak longwave infrared focal plane module (FPM) temperature. The temperature on the Y-axis is the operating temperature of the ABI focal plane. During the pre- and post-equinox seasons, the sun is in the right position to heat up the focal plane, causing channel saturation that shows up as striping and noise in the imagery.

Much progress has been made to optimize the performance of the GOES-17 data and the instrument is currently delivering 97% of the data it was intended to provide. From the perspective of the LST product, efforts have been devoted to the development of an alternative algorithm applicable to sensor data during the "hot" period. Such an algorithm is expected to improve the product quality and availability.

Impacts of the FPM temperature to sensor data from different channels are different (Table 3.5). The design of the mitigation algorithm is to swap the band 15 used by the enterprise algorithm with a channel which is less impacted by the FPM temperature.

Table 3.5. Estimated GOES-17 ABI channel availability.

Band	Channel	Estimated Unsaturated Signal Cold Season (Solstice)	Estimated Unsaturated Signal Warm Season (Pre-Eclipse)
1	0.47 µm	24 hr	24 hr
2	0.64 µm	24 hr	24 hr
3	0.86 µm	24 hr	24 hr
4	1.38 µm	24 hr	24 hr
5	1.61 µm	24 hr	24 hr
6	2.25 µm	24 hr	24 hr
7	3.90 µm	24 hr	24 hr

8	6.18 μm	24 hr	18 - 20 hr
9	6.95 μm	24 hr	18 - 20 hr
10	7.34 μm	24 hr	18 - 20 hr
11	8.50 μm	24 hr	21 hr
12	9.61 μm	24 hr	18 - 20 hr
13	10.35 μm	24 hr	24 hr
14	11.20 μm	24 hr	24 hr
15	12.30 μm	24 hr	21 hr
16	13.30 μm	24 hr	18 - 20 hr

A comprehensive evaluation and analysis leads to the combination of bands 13 and 14, while the retrieval formula remains as the enterprise algorithm (Eq. 3.6).

$$T_s = C + A_1 T_{10} + A_2 (T_{10} - T_{11}) + A_3 \varepsilon + A_4 \varepsilon (T_{10} - T_{11}) + A_5 \Delta\varepsilon \qquad (3.6)$$

where T_{10} and T_{11} represent the top-of-atmosphere brightness temperatures at ~10 μm and ~11 μm, respectively, $\varepsilon = 0.5 * (\varepsilon_{10} + \varepsilon_{11})$ and $\Delta\varepsilon = (\varepsilon_{10} - \varepsilon_{11})$ are the average and difference of the spectral emissivity of the land surface at ~10 μm and ~11 μm, respectively, θ is the satellite view zenith angle, and $C,\ A_1,\ A_2,\ A_3,\ A_4,\ D$ are the algorithm coefficients, stratified by day/night and different atmospheric conditions.

A prescribed FPM temperature threshold value is used to determine whether enterprise or mitigation algorithm is used for LST retrieval, *i.e.*, if the FPM temperature is lower than the given threshold value, the enterprise algorithm will be used, and the mitigation algorithm will be adopted otherwise. Note that the same algorithm will be applied to the retrieval of the whole satellite scene at any given time for better spatial consistency.

3.4.3 Algorithm Output

Three LST products are generated corresponding to three ABI scan coverages, CONUS, Mesoscale, and FD. Output of the LST products mainly contain three data arrays: the LST values, the data quality flags (DQF), and the product quality information (PQI) flags. To minimize storage request of the LST product, the LST value is stored in a short integer using the following scaling equation:

$$T_s = T_{int} \times scaling\_factor + offset \qquad (3.7)$$

where T_{int} is the integer from the retrieved LST, T_s. The scaling_factor and offset values can be found in the variable attributes.

The PQI flags are 2-byte bitwise short integer, which contains quality information of LST production for each pixel. In addition, a similar set of quality control (QC) flags is required for operational monitoring purpose. The LST values and quality flags data arrays are described in Table 3.6.

Table 3.6. Algorithm output data.

Name	Type	Description	Dimension
LST values	Short Integer	Retrieved land surface temperature value for each pixel of the scanning mode. Scaling factor is 100, offset is 10000, corresponding to Eq (3.7).	grid (xsize, ysize)
Product Quality Information (PQI) flags	Short Integer	Bit-based product quality information for each pixel of the scanning mode: Land, cloudiness, sensor data quality, day/night, dry/moist, very moist, large view zenith, very cold surface, etc.	grid (xsize, ysize)
Data Quality flags (DQF)	Short Integer	Bit-based quality control flags for each pixel of the scanning mode	grid (xsize, ysize)

The PQI is comprised of a total of 16 bits holding the test results (yes/no) for each of the various tests and flags. Such information is designed to help users in their applications. The DQF is solely related to the quality of the LST product, with 0 indicating good quality, 1 indicating medium, 2 indicating low, and 3 indicating no retrieval. Details of the LST PQI can be found in Table 3.7 and the DQF flags are defined in Table 3.8. Table 3.9 gives the definition of LST Quality.

Table 3.7. Product quality information flags of the full resolution LST product.

Byte	Bit	Flag	Source	Effect
1	1-0	LST Quality	LST	00=high, 01=medium, 10=low, 11=no retrieval
	3-2	Cloud Condition	Cloud Mask	00=clear, 01=probably clear, 10=probably cloudy, 11= cloudy
	4	Input Data Quality	SDR & Other Input	0=normal, 1=output of space, bad data, or missing data
	5	AOD at 550 nm (slant path)	AOD	0=within range(AOD<=1.0); 1=out of range (AOD >1) or missing
	7-6	Land Surface Cover	Land/Sea & Snow/Ice Mask	00=land;01=snow/ice;10=in land water;11=coastal
2	1-0	Water vapor condition	TPW	00=very dry (wv<1.5g/cm^2); 01= dry [1.5, 3); 10=moist [3, 4.5); 11= very moist [4.5+)
	2	Emissivity Availability	Emissivity	0=AWG emissivity, 1=Other
	3	View Angle	SDR	0=normal, 1=large view angle (>55 deg)
	4	Day/night	SDR	0=night (solar zenith > 85deg), 1=day (solar zenith <= 85 deg)
	5	Thin cirrus	Cloud Mask	0= no cirrus, 1= cirrus
	6	Fire contamination	Cloud mask	0= no , 1= yes
	7	Reserved		Reserved for future use

Note: No retrieval of AOD and thin cirrus during nighttime. LST Quality does not depend on AOD and thin cirrus when they are not retrieved.

*In case 01 (snow/ice) and 10 (in-land water) coexist, surface type will be set to 01 (snow/ice)

Table 3.8. Data quality flags of the full resolution LST product.

Byte	Bit	Flag	Source	Effect
1	1-0	LST Quality	LST	00=high, 01=medium, 10=low, 11=no retrieval
	2-7	Empty		Reserved for future use
2	0-7	Empty		Reserved for future use

Table 3.9. Definition of LST Quality in PQI and DQF.

Valid LST	View Angle	Fire	AOD in range (Available)	Thin Cirrus (Day)	Cloud Index		
					Clear	Probably Clear	Probably Cloudy
yes	x	x	x	yes	Low	Low	Low
yes	x	x	no	x	Low	Low	Low
yes	x	yes	yes	x	Low	Low	Low
yes	>55	no	yes	no	Medium	Medium	Low
yes	<=55	no	yes	no	High	Medium	Low
no	x	x	x	x	No Retrieval	No Retrieval	No Retrieval

Note: x: indifferent

AOD is not retrieved under nighttime, snow/ice surface, cloud, etc. If there is no AOD retrieval, the AOD range criteria will be excluded in above matrix. Similarly because thin cirrus detection is only available at daytime, it is excluded in above matrix for nighttime pixel LST quality determination.

In addition to the pixel level LST values, PQI and quality control flags, metadata are needed in the LST product describing the common and LST specific information about the product. The GOES-R AWG and the Land Team recommend that the following metadata (Table 3.10) should be included in the ABI LST products.

Table 3.10. Metadata defined for the LST product file.

METEDATA	TYPE	DEFINITOIN
flag_mitigation	common	0: enterprise; 1: mitigation
max_LST	common	Maximum LST within valid range
min_LST	common	Minimum LST within valid range
mean_LST	common	Mean LST within valid range
standard_deviation _LST	common	Standard deviation of LST within valid range
count_space	common	Count of pixels with space view
count_land	common	Count of pixels on land, including those with no LST retrievals
count_retrieved	common	Count of pixels with LST retrievals, including those beyond valid range

count_within_range	common	Count of pixels with LST within valid range
count_clear	common	Count of LST retrievals with clear condition
count_probably_clear	common	Count of LST retrievals with probably clear condition
count_high_quality	common	Count of LST retrievals with high quality
count_medium_quality	common	Count of LST retrievals with medium quality
count_low_quality	common	Count of LST retrievals with low quality
count_large_angle	common	Count of LST retrievals with large view angle

It is noted that LST values is not calculated for pixels indicated as cloudy, bad/out of space/missing data, and ocean. Inland water pixel is considered as land pixel and the LST over such a pixel will be calculated.

4 TEST DATASETS AND OUTPUTS

The selected algorithm (10) is evaluated by validation with in-situ LST measurement. All following references in this section to "the algorithm" will refer to algorithm 10.

4.1 Enterprise LST Test Outputs

The enterprise algorithm was applied to data from both GOES-16 and GOES-17. Some of the required input are not available yet, *e.g.*, enterprise cloud mask, enterprise TPW. The primary sensor data are available from the existing baseline processing system. Major derived sensor data, including enterprise cloud mask, TPW, AOD, snow/ice mask are not available and replaced by their baseline counterparts. It is assumed that this will not significantly impact the quality of the enterprise LST product. Emissivity data used for this test is the MODIS emissivity monthly climatology currently being used in the baseline algorithm. The LUT is stratified by TPW, satellite view zenith angle, and day/night conditions. Figure 4.1 shows an example of the enterprise LST output from GOES-East.

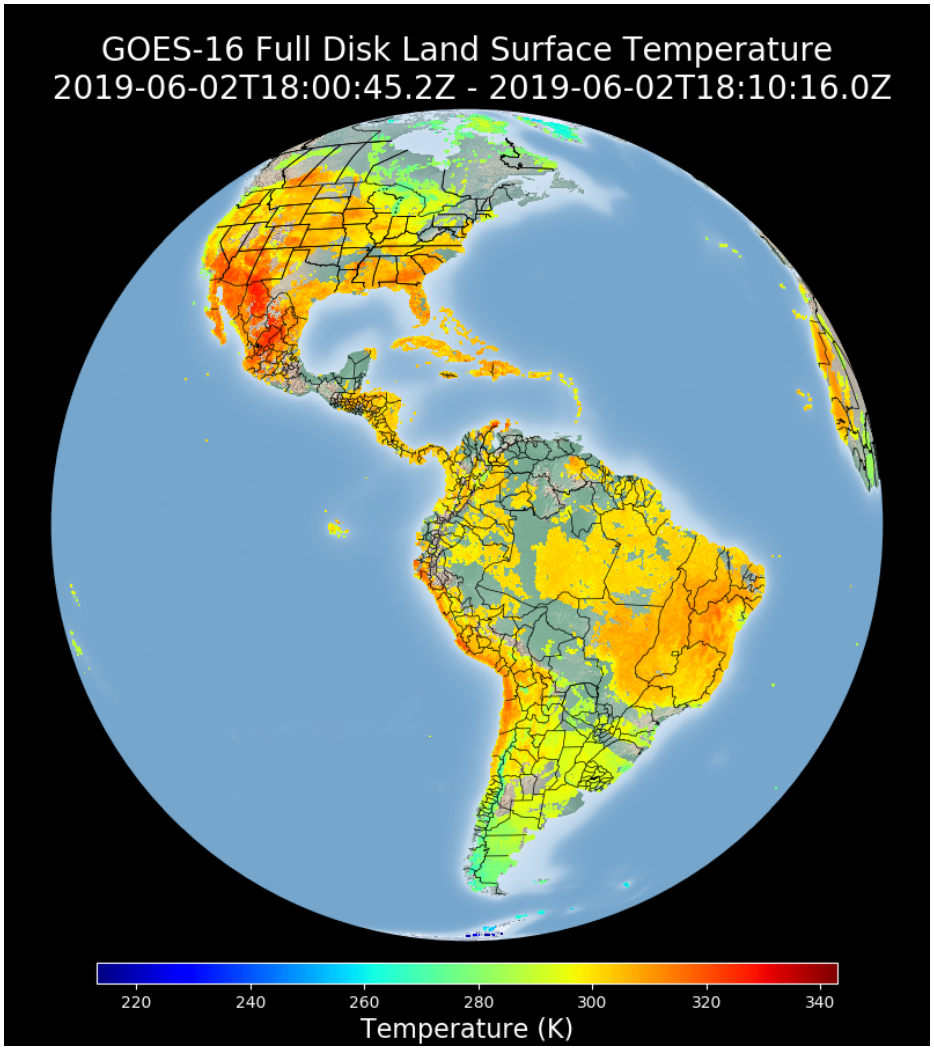

Figure 4.1. Example GOES-16 Full Disk enterprise LST output.

4.2 Validation with SURFRAD In-situ Measurement

4.2.1 SURFRAD data

Though challenging, remotely sensed LST must be validated Traditionally, LST validation is carried out via its direct comparison to in-situ LST measurements [Yu et. al, 2012]. Multiple factors can have significant impacts on the validation. Compared to the 2 km resolution of CONUS and MESO LSTs and 10 km resolution of FD LST, the ground station usually observes an area within a few tens of meters. The mismatch of the field of view requires that the in-situ station site is homogeneous enough to well represent a satellite pixel. This is rarely the case since LST usually has very large spatial variability. Moreover, a good estimate of the broadband surface emissivity is needed to evaluate the in-situ LST measurement. Due to its rapid temporal variation, in-situ LST measurements must be well matched in time to the satellite counterpart. A comprehensive LST validation is impossible unless these problems can be solved.

Based on the above factors, the National Oceanic and Atmospheric Administration's (NOAA) Surface Radiation budget (SURFRAD) network (Yu et al, 2012; Augustine & Dutton, 2013) is selected for the validation of GOES-R LST. It is the first U.S. national-scale network to continuously measure the land surface radiation budget since 1995. It includes seven long-term observation stations (Figure 4.2) and covers a variety of different land surface types, including evergreen-broadleaf-forest, deciduous-broadleaf-forest, mixed-forest, closed-shrubland, open-shrubland (desert), woody-savanna, grassland, cropland, crop-mosaic, snow, and barren/desert.

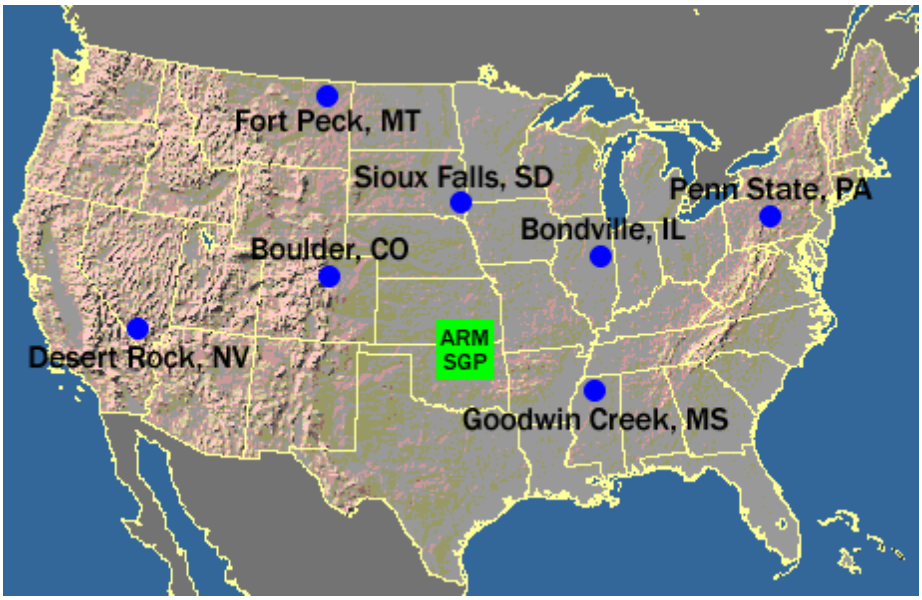

Figure 4.2. Distribution of SURFRAD stations in the CONUS.

SURFRAD provides in-situ measurements of downwelling and upwelling infrared radiation, along with other meteorological parameters [Augustine et al., 2005]. Due to its high quality, existence of long-term time series, and systematic reliability, the data have been extensively used to support satellite system validation, numerical model verification, and modern climate, weather, and hydrology research applications.

SURFRAD LST is derived from the upwelling and downwelling radiation. The observed upwelling ($F^{\uparrow}$) and downwelling ($F^{\downarrow}$) radiative fluxes are converted to temperature as follows:

$$F^{\uparrow} = \varepsilon\sigma T_s^4 + (1-\varepsilon)F^{\downarrow} \quad (4.1)$$

where ε is the broadband surface emissivity and σ is the Stefan-Boltzman constant (σ= $5.67051\text{x}10^{-8}$ $\text{Wm}^{-2}\text{k}^{-4}$). The station LST is then calculated using the following equation:

$$T_s = \left[\frac{F^{\uparrow} - (1-\varepsilon)F^{\downarrow}}{\varepsilon\sigma}\right]^{\frac{1}{4}} \quad (4.2)$$

A daily emissivity product has been developed by the GOES-R LST Algorithm Working Group (AWG) to evaluate the in-situ LST.

4.2.2 Match-up GOES-16 and GOES-17 Data with SURFRAD

Data from both GOES-16 and GOES-17 were collected since operational products from the two are available. The enterprise algorithm was applied to the CONUS data from both satellites. The GOES-16 LST from 12/14/2017 to 8/31/2019 and the GOES-17 LST from 8/12/2018 to 8/31/2019 were used for the validation with the in-situ measurements.

The satellite LST is matched to the in-situ observations in both time and space. The maximum differences are one minute in time and 0.02º in space, respectively. Since LST variability in time and space can be very large, the satellite pixel size and the temporal output period are used as the maximum spatial difference and temporal difference, respectively, in order to obtain the closest matchup between the satellite product and its in-situ counterpart. To ensure the best comparison quality, an effective cloud filtering is needed. In baseline processing system, the four-level cloud mask information, clear, probably clear, probably cloudy, and cloudy, were included in the cloud mask intermediate product (IP), which was not available for a significant amount of time. Only two-level cloud mask information, clear (including clear and probably clear) and cloudy (including probably cloudy and cloudy), can be used in filtering out the cloudy matchups. To reduce the potential cloud contamination and to obtain more objective validation results, a simplified multi-step additional cloud filtering procedure was used after the application of the two-level baseline cloud mask. The matchup is determined as being potentially impacted by cloud if any of the following three criteria satisfies:

1) If any neighboring pixel (3x3 box centered at the matchup pixel) is flagged as cloudy;
2) If the standard deviation of the band 14 brightness temperature in the neighboring 3x3 pixel box is larger than a threshold value;
3) If the standard deviation of the 30-minute (centered at the matchup time) downwelling radiation from in-situ observations is higher than a predetermined threshold value.

4.2.3 Validation Results and Analysis

Figure 4.3 shows the validation results of the enterprise LST from both GOES-16 and GOES-17 with SURFRAD in-situ measurements. As a reference the corresponding baseline LST validation results are also included.

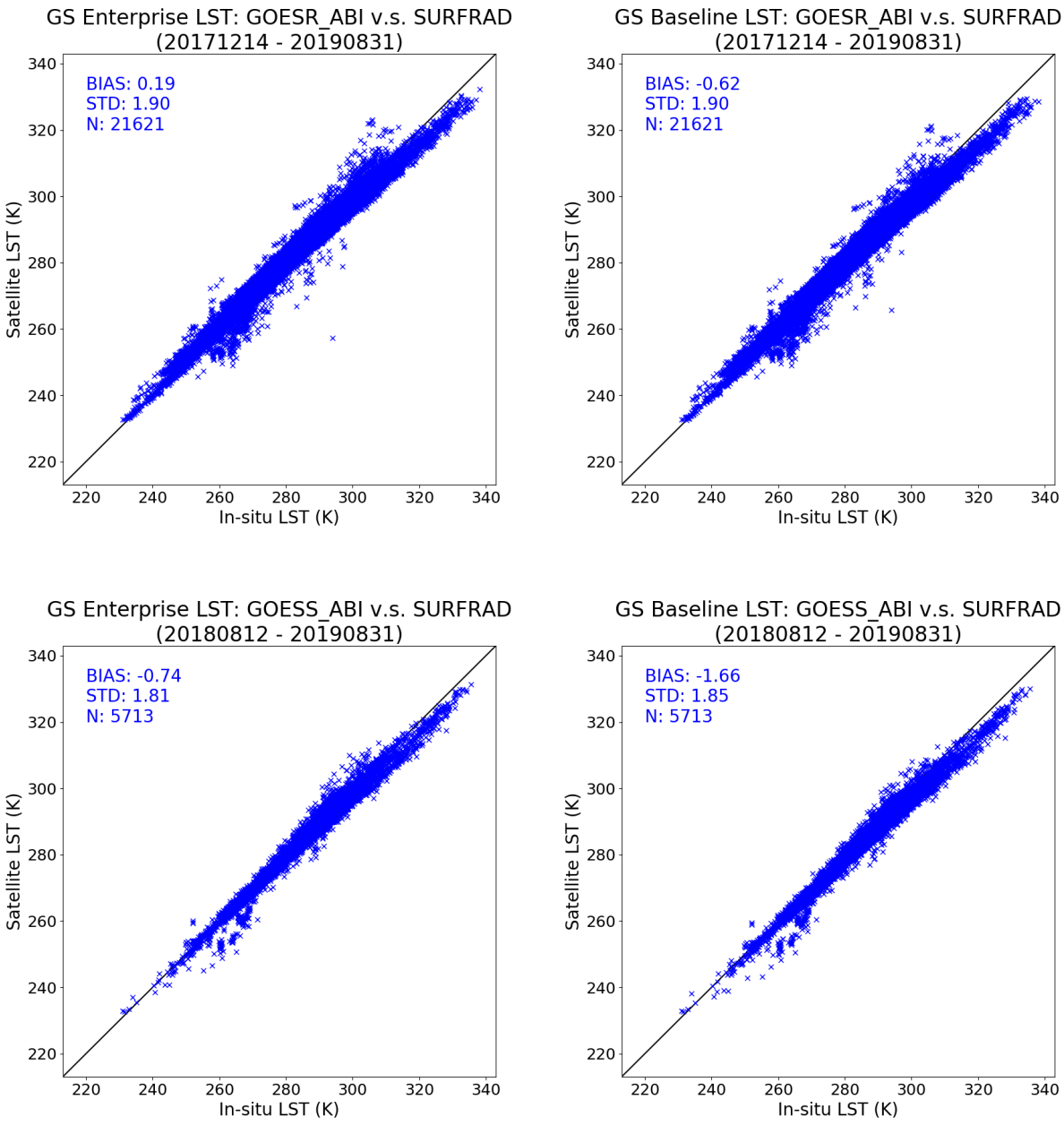

Figure 4.3. LST validation results of enterprise GOES-16 (upper left), baseline GOES-16 (upper right), enterprise GOES-17 (lower left), and baseline GOES-17 (lower right).

The enterprise algorithm is able to outperforms the baseline algorithm in retrieval bias from both GOES-16 and GOES-17. The detailed statistics for each site can be found in Tables 4.1 and 4.2 for GOES-16 and GOES-17, respectively.

Table 4.1. Validation results of enterprise and baseline GOES-16 LSTs with each SURFRAD site.

Site	Number	Enterprise LST		Baseline LST	
		Accuracy (K)	Precision (K)	Accuracy (K)	Precision (K)
Bondville	3227	1.16	2.05	0.24	2.08
Boulder	3161	-0.44	1.59	-1.14	1.60
Desert Rock	3275	-2.63	1.84	-3.54	1.83
Fort Peck	2937	-0.32	1.88	-1.01	1.95
Goodwin Creek	3566	1.59	1.78	0.61	1.76
Penn State	1995	1.80	2.26	1.14	2.17
Sioux Falls	3460	0.62	1.96	-0.16	1.99

Table 4.2. Validation results of enterprise and baseline GOES-17 LSTs with each SURFRAD site.

Site	Number	Enterprise LST		Baseline LST	
		Accuracy (K)	Precision (K)	Accuracy (K)	Precision (K)
Bondville	395	1.41	1.94	0.38	1.98
Boulder	1375	-0.35	1.28	-1.08	1.36
Desert Rock	1736	-2.41	1.73	-3.48	1.74
Fort Peck	1314	-0.81	2.20	-1.57	2.28
Goodwin Creek	383	1.18	2.41	-0.04	2.41
Penn State	134	1.78	1.61	0.77	1.63
Sioux Falls	376	0.71	1.40	-0.30	1.54

The validation results are quite consistent between GOES-16 and GOES-17, where the performance of the enterprise algorithm at relatively dry site, *e.g.*, Boulder, Desert Rock, Fort Peck, is significantly better than the baseline algorithm. This is particularly the case for Desert Rock site, at which the significant underestimate by baseline algorithm (around 3.5 K in both GOES-16 and GOES-17) was reduced by ~1 K with the enterprise LST results. More analysis is needed to improve the performance of the enterprise algorithm at more vegetated areas.

4.3 Mitigation Algorithm Evaluation

The mitigation algorithm was applied to the GOES-17 data and compared to the SURFRAD in-situ measurement (Figure 4.4). It is found that the LST for both daytime and nighttime are able to meet the mission requirement. Table 4.3 lists the detailed comparison results with each of the SURFRAD sites. It is worth mentioning that the mitigation algorithm works extremely well at Desert Rock site, whose underestimate is reduced to around 1 K.

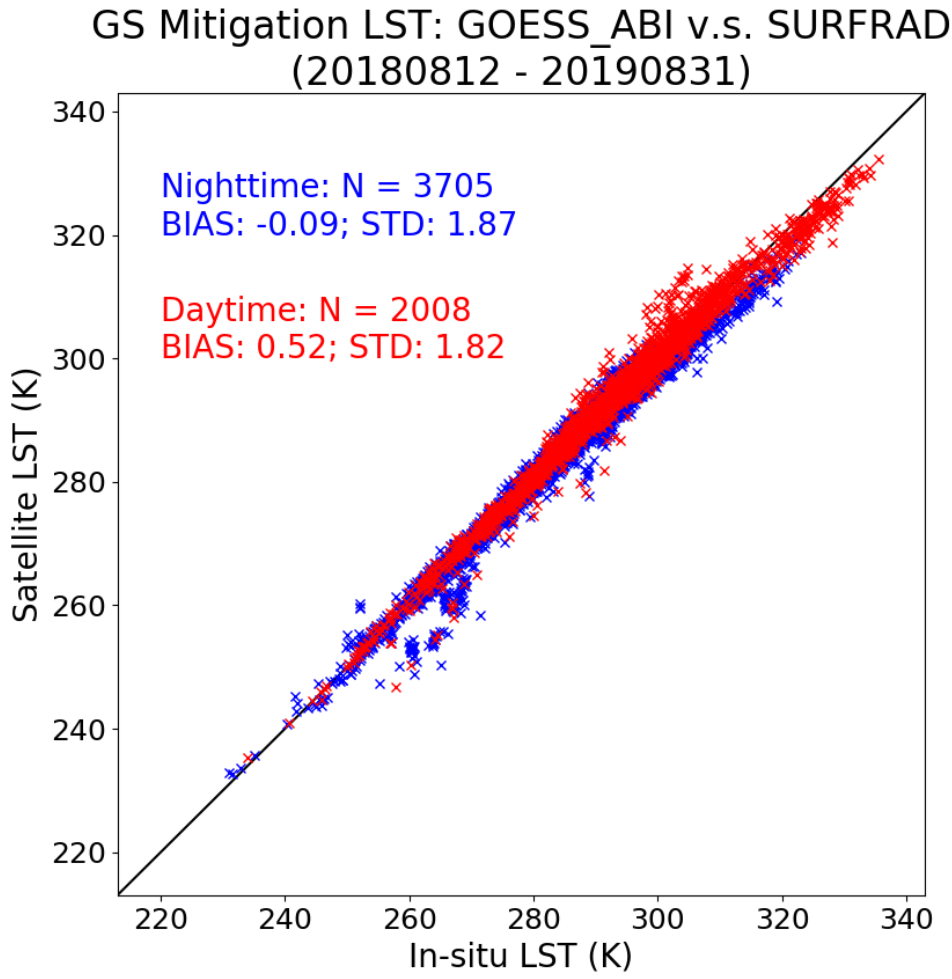

Figure 4.4. GOES-17 mitigation LST validation results with SURFRAD in-situ observations.

Table 4.3. Validation results of mitigation GOES-16 LSTs with each SURFRAD site.

Site	Number	Accuracy (K)	Precision (K)
Bondville	395	2.28	2.03
Boulder	1375	0.38	1.31
Desert Rock	1736	-1.01	1.78
Fort Peck	1314	-0.19	2.31
Goodwin Creek	383	1.35	2.11
Penn State	134	2.50	1.65
Sioux Falls	376	1.13	1.58

In order to analyze the performance of the algorithm with different FPM temperature, the GOES-17 data on August 22, 2019 was used to compare its GOES-16 counterpart (Figure 4.5). During the course of this day, the FPM temperature changes from 81 K to as high as 105 K. In this comparison, the GOES-16 LST was projected to the GOES-17 grids.

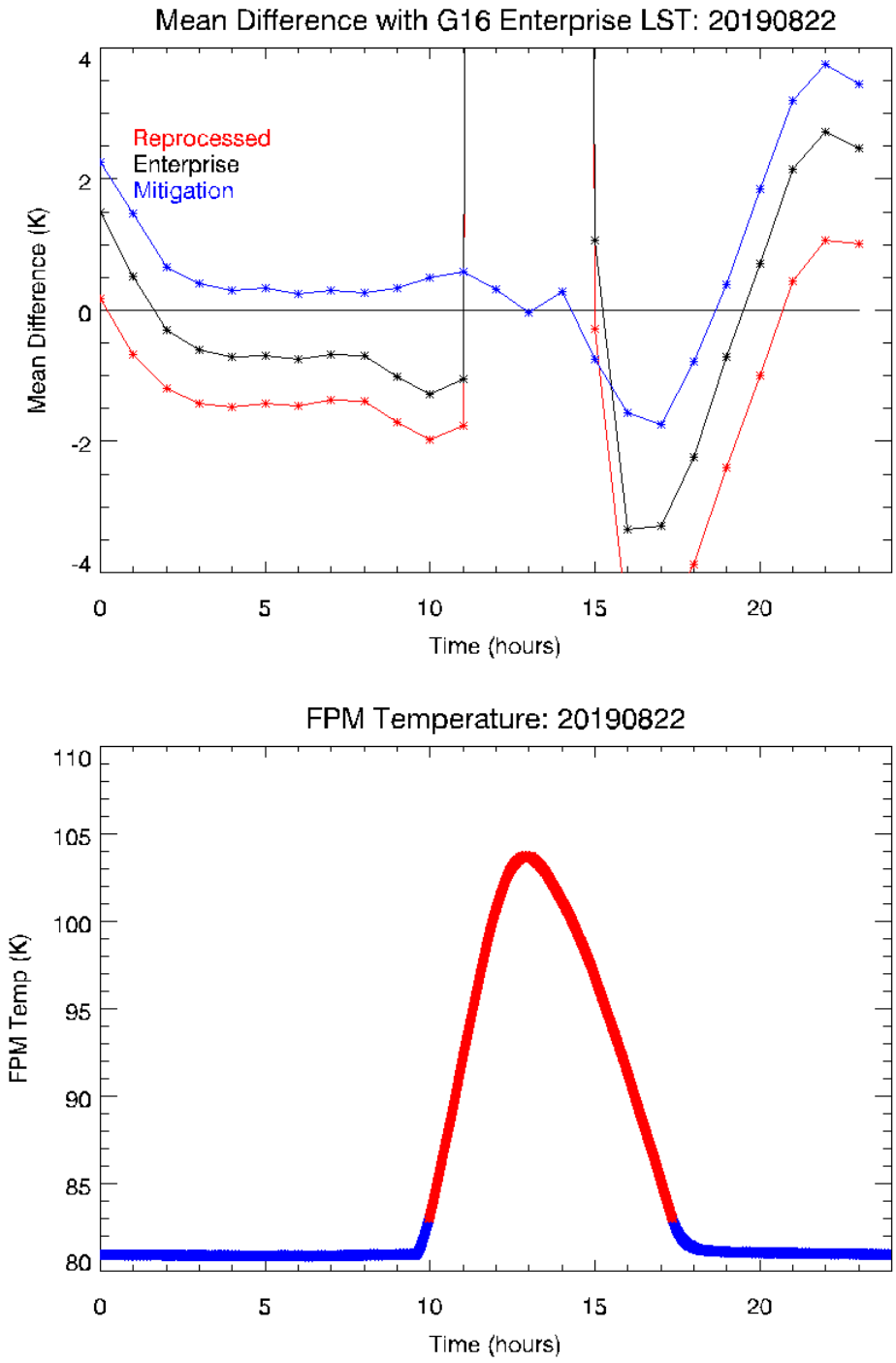

Figure 4.5. upper: mean difference of reprocessed baseline (red), enterprise (black), and mitigation (blue) LSTs with the corresponding GOES-16 LST; lower: the FPM temperature evolution of the day.

It is observed that the GOES-17 enterprise LST is closer to the GOES-16 LST throughout the day. When FPM temperature is relatively low, the mitigation LST performs slightly worse than or similar to the enterprise LST. When FPM temperature is high, *e.g.*, beyond 90 K, both

enterprise and baseline LSTs significantly differ from the GOES-16 LST, while the mitigation LST is stably close to the latter.

The above analyses show the potential advantages by using the mitigation algorithm when FPM temperature is high. However, at the time of this analysis, we do not have access to the upstreaming input data of the mitigation version. More analysis is needed when all necessary input is ready.

4.4 Error Budget

In the algorithm evaluation process, as mentioned earlier, there are several issues that should be further studied in the match-up dataset comparisons. Difference between the satellite pixel-size measurement and the ground spot-size measurement must be characterized for a high quality validation procedure. More accurate broadband emissivity values are needed to better estimate the ground LSTs.

Cloud contamination is still a problem even if we have used a stringent cloud filtering procedure in generating the match-up dataset. It is found that a little threshold value or procedure change will have significant impact to the output match-up data pairs, though the overall validation results are not obviously affected.

All the above factors may potentially degrade the algorithm performance when it is applied for the real GOES-R satellite data.

5 PRACTICAL CONSIDERATIONS

5.1 Numerical Computation Considerations

The LST algorithm selected is mathematically simple, and requires no complicated mathematical routines. In operations it will be robust and fast enough in terms of the algorithm latency requirement (< 15 minutes, goal) using current computer power. There is no specific numerical computation requirement needed. For storage consideration, LST values should be saved in two-byte integers, with scale factors (intercept and slope) defined for the entire dataset. Quality flags for each pixel value should be bit-flag definitions, to minimize data storage.

5.2 Programming and Procedural Considerations

The LST algorithm is a pixel-by-pixel algorithm, implemented in sequential mode. Because of the algorithm simplicity, it requires small amount of code, with basic mathematical routines. However, since the LST algorithm requires ancillary datasets such as emissivity data and the total column atmospheric water vapor data, pre-calculated lookup tables may be needed for mapping the ancillary datasets to the ABI pixel geolocation. Besides, the algorithm processing routines should be programmed in block functions for integration ease.

Due to the algorithm coefficients clarification for difference atmospheric conditions (day/night, dry/moist), spatial discontinuity of the derived LST field is a concern, though such discontinuity is not obvious in the proxy data tests. Further verification should be performed to ensure it is not a real problem.

5.2.1 Configuration of Retrieval

The primary adjustable parameters for the LST retrieval are the algorithm coefficients that are stratified for different atmospheric conditions and satellite view angles. Number of stratifications and criterion values for these conditions should be adjustable in order to optimize the algorithm if needed. Source of ancillary datasets should be configurable for the best dataset. And finally, it should be kept in mind that metadata used for the product may be modified, reduced and added in later phase of the product generation.

5.3 Quality Assessment and Diagnostics

The LST retrieval will be assessed and monitored. First, a set of quality control flags will be generated with the LST product for retrieval diagnostics, as is presented in Section 3.4.3. The quality control flags will indicate the retrieval conditions, including the land/non-land surfaces (i.e., ocean, snow, ice, water etc.), atmospheric water vapor status (i.e., dry, moist and very moist conditions), day and night, large view angle, very cold surface, etc. Details are shown in Table 3.7. LST maps and statistical information will be generated and reviewed for quality assessment.

5.4 Exception Handling

The algorithm will handle exceptions through the quality control flags. In calculating the LST for each pixel, quality control flags from input datasets will be examined for bad sensor data (e.g., missing or no sensor data). Pixels with space view will be skipped. Availability of other ancillary datasets such as emissivity and water vapor will also be checked. When the necessary input data is not available, the retrieval will be skipped, however, the corresponding quality flags will still be processed to indicate the type of the exception.

In case the ABI derived sensor data are used as input to the LST algorithm, if the ABI snow mask, land surface emissivity, and TPW are not available, alternative ancillary data should be checked first for LST algorithm input before the LST calculation is skipped.

5.5 Algorithm Validations

Near-real-time validation and monitoring of the baseline LSTs from GOES-16 and GOES-17 is being conducted, including the visualization component, the data verification component, and a weekly routine validation module. These are being automatically run since the beginning of the LST products from both satellites. The system is designed not only to monitor the product and ensure its long-term stability, but also to accumulate long time series of data with in-situ measurement for algorithm improvement. This dataset plays a crucial role in the enterprise algorithm development, selection, and improvement. It will be adapted to the enterprise LST once it is in operation.

6 ASSUMPTIONS AND LIMITATIONS

The following sections describe the limitations and assumptions used in the current version of the LST.

6.1 Assumed Algorithm Performance

The following assumptions have been made in developing and estimating the performance of the LST retrieval algorithm and products, including proposed mitigation strategies in parentheses.

- The ABI cloud mask is available at the time of LST retrieval (Use alternative built-in algorithm to identify cloudy pixels),
- High quality dynamic ABI land surface emissivity dataset is available (Use the monthly mean emissivity from the CIMSS baseline fit emissivity database as an alternative),
- ABI baseline TPW dataset is available (Use the NCEP analysis and forecast water vapor dataset).
- ABI brightness temperature data in channels 14 and 15 are available, calibrated and navigated, and are not distorted (set quality flag to bad pixels and no LST retrieval is performed).
- Even with the mitigation algorithm, degradation of the product is expected when the FPM temperature is high.

The LST retrieval algorithm is applicable only on cloudless pixels. LST effects due to roughness and/or structure of land surface, the emissivity directional feature and its variation in a pixel are not handled in the algorithm. The retrieved LST value is an effective land surface skin temperature over isothermal mixed pixel. The retrieval accuracy may be reduced significantly in regions with heavy atmospheric water vapor loading (e.g. > 5.0 g/cm^2). Also, the retrieval may be questionable in regions with very low LST and where the surface air temperature is higher than LST.

6.2 Assumed Sensor Performance

It is assumed that the GOES-R ABI sensor will meet its specifications as documented in the ABI Performance Operational Requirements Document (PORD) (417-R-ABIPORD-0017). In case the sensor performance is not met, the performance of LST algorithm may be affected, with an uncertainty in meeting the product requirement. With the LHP overheating issue, degradation of the product and reduction of the data availability are expected when the FPM temperature is high even with the mitigation algorithm.

6.3 Potential Improvements

The large diurnal variability of LST is something conceptually understood, but poorly described quantitatively and not explicitly accounted for in the algorithm. The amplitude of the diurnal cycle is determined by surface cover, specifically the green vegetation fraction and soil moisture. The Bowen ratio over bare dry soil is high and over transpiring vegetation is low, and therefore green vegetation fraction in each pixel is important to LST and its diurnal range, with diurnal

variation much larger in low vegetation pixels. A second contributor to LST variation is the fraction of surface shadowing seen from the observing satellite. This effect arises because shaded surfaces are significantly cooler than sunlit surfaces, so the apparent shadow fraction in a pixel is important. It, of course, varies according to the relative geometry of the sun and satellite and is changing throughout daylight hours. All of these factors should be factored into the LST algorithm and work on that problem is planned.

In addition, we are working on an inversion method that can derive the LST and the surface emissivity simultaneously using multi-channel and multi-observation measurements. Originally, such method was applied to the EOS/MODIS mission through its day and night observations over a pixel (Wan, 2008). The method can be applied to GOES-R ABI data better since it provides multiple observations over a pixel in a short time interval, which ensures constant emissivity during the time which is the baseline of the inversion method. We simplified the method significantly and have had the output stable and faster (Yu et al., 2009d).

7 REFERENCES

Atitar, M. and J. A. Sobrino, 2008: A Split-Window Algorithm for Estimating LST From Meteosat 9 Data: Test and Comparison With In Situ Data and MODIS LSTs, *IEEE Geosci. Remote Sens. Lett.*, **6(1)**, pp. 122-126, doi: 10.1109/LGRS.2008.2006410

Augustine, J. A. and Dutton E. G., 2013: Variability of the surface radiation budget over the United States from 1996 through 2011 from high-quality measurements. *J. Geophys. Res.-Atmos.*, **118**, 43–53, doi: 10.1029/2012JD018551

Baker N., 2013: Land Surface Temperature Visible/Infrared Image radiometer Suite Algorithm Theoretical Basis Document, http://www.star.nesdis.noaa.gov/jpss/documents/ATBD/D0001-M01-S01-022_JPSS_ATBD_VIIRS-LST_A.pdf

Becker, F. and Z. L. Li, 1990: Towards a local split window method over land surfaces, *Int. J. Remote Sens.*, **11(3)**, pp. 369-393, doi: 10.1080/01431169008955028

Borbas, E. E., L. Moy, S. W. Seemann, R. O. Knuteson, P. Antonelli, J. Li, H-L Huang, L. Trigo, I. de Meteorologia, and L. Zhou, 2008: A Global Infrared Land Surface Emissivity Database and Its Validation, P2.7, *AMS Annual meeting,* New Orleans, January, 2008.

Berk, A., G. P. Anderson, P. K. Acharya, J. H. Chetwynd, M. L. Hoke, L. S. Bernstein, E.P. Shettle, M.W. Matthew, and S. M. Alder-Golden, 2000: MODTRAN4 Version 2 Users's Manual, Space Vehicles Directorate, Hanscom AFB, MA 01731-3010, April 2000.

Berk, A., G. P. Anderson, P. K. Acharya, L. S. Bernstein, L. Muratov, J. Lee, M. J. Fox, S. M. Adler-Golden, J. H. Chetwynd, M. L. Hoke, R. B. Lockwood, T. W. Cooley, and J. A. Gardner, 2005: MODTRAN5: a Reformulated Atmospheric Band Model with Auxiliary Species and Practical Multiple Scattering Options, *Proc. SPIE Int. Soc. Opt. Eng*. 5655, 88 (2005).

Caselles, V., C. Coll, and E. Valor, 1997: Land surface temperature determination in the whole Hapex Sahell area from AVHRR data, *Int. J. Remote Sens.*, **18(5)**, pp. 1009–1027, 1997.

Chédin, A. and N. A. Scott, 1985: The impact of spectroscopic parameters on the composition of the Jovian atmosphere discussed in connection with recent laboratory, earth and planetary observation programs. *J. Quant. Spectrosc. Radiat. Transfer* **32(5-6)**, pp. 453-461, doi: 10.1016/0022-4073(84)90040-2

Chevallier, F., F. Chéruy, N. A. Scott, and A. Chédin, 1998: A neural network approach for a fast and accurate computation of longwave radiative budget. *J. Appl. Meteorol.*, **37(11)**, pp. 1385-1397, doi: 10.1175/1520-0450(1998)037<1385:ANNAFA>2.0.CO;2

Coll, C., E. Valor, T. Schmugge, and V. Caselles, 1997: A procedure for estimating the land surface emissivity difference in the AVHRR channels 4 and 5, Remote Sensing Application to the Valencian Area, Spain.

Coll, C., V. Caselles, J. M. Galve, E. Valor, R. Niclòs, J. M. Sanchez, and R. Rivas, 2005: Ground measurements for the validation of land surface temperatures derived from AATSR and MODIS data, *Remote Sens. Environ.*, **97(3)**, 288–300, 10.1016/j.rse.2005.05.007

Coll, C., J. M. Galve, J. M. Sanchez, and V. Caselles, 2010: Validation of Landsat-7/ETM+ thermal-band calibration and atmospheric correction with ground-based measurements, *IEEE Trans. Geosci. Remote Sens.*, **48(1)**, 547–55, doi: 10.1109/TGRS.2009.2024934

Coll, C., E. Valor, J. M. Galve, M. Mira, M. Bisquert, V. García-Santos, F. Caselles, and V. Caselles, 2012: Long-term accuracy assessment of land surface temperatures derived from the Advanced Along-Track Scanning Radiometer, *Remote Sens. Environ.*, **116(15)**, 211–225, doi: 10.1016/j.rse.2010.01.027

Ellrod, G. P., 1998: Detection and analysis of fog at night using GOES multispectral infrared imagery, *NOAA Tech. Rep.* NESDIS 75, 22 pp.

Fang, L., X. Zhan, M. Schull, S. Kalluri, I. Laszlo, P. Yu, C. Carter, C. Hain, M. Anderson, 2019: Evapotranspiration Data Product from NESDIS GET-D System Upgraded for GOES-16 ABI Observations, *Remote Sens.*, **11(22)**, doi: 10.3390/rs11222639

Galve, J.M., C. Coll, V. Caselles, and E. Valor, 2008: An Atmospheric Radiosounding Database for Generating Land Surface Temperature Algorithms, *IEEE Trans. Geosci. Remote Sens.*, **46(5)**, pp. 1547-1557, doi: 10.1109/TGRS.2008.916084

Global Climate Observing System, 2017: GCOS Implementation Plan 2016 – The Global Observing System for Climate: Implementation Needs.

Göttsche F., F. Olesen, I. F. Trigo, A. Bork-Unkelbach, and M. A. Martin, 2016: Long Term Validation of Land Surface Temperature Retrieved from MSG/SEVIRI with Continuous in-Situ Measurements in Africa, *Remote Sens.*, **8(5)**, doi: 10.3390/rs8050410

Guillevic, P. C., J. L. Privette, B. Coudert, M. A. Palecki, J. Demarty, C. Ottlé, and J. A. Augustine, 2012: Land Surface Temperature product validation using NOAA's surface climate observation networks-Scaling methodology for the Visible Infrared Imager Radiometer Suite (VIIRS). *Remote Sens. Environ.*, **124**, pp. 282–298, doi: 10.1016/j.rse.2012.05.004

Hillger, D. and P. Gary, 2003: Detection of Important Atmospheric and Surface Features by Employing Principal Component Image Transformation of GOES Imagery, *J. Appl. Meteorol.*, **42(5)**, pp. 611–629, doi: 10.1175/1520-0450(2003)042<0611:DOIAAS>2.0.CO;2

Hook, S. J., R. G. Vaughan, H. Tonooka, and S. G. Schladow, 2007: Absolute radiometric in-flight validation of mid infrared and thermal infrared data from ASTER and MODIS on the Terra spacecraft using the Lake Tahoe, CA/NV, USA, Automated Validation Site. *IEEE Trans. Geosci. Remote Sens.*, **45(6)**, pp. 1798–1807, doi: 10.1109/TGRS.2007.894564

Hulley, G. C. and S. J. Hook, 2009: The North American ASTER Land Surface Emissivity Database (NAALSED) Version 2.0. *Remote Sens. Environ.*, **113(9)**, pp. 1967–1975, doi: 10.1016/j.rse.2009.05.005

Hulley, G., N. Malakar, T. Hughes, and S. Hook, 2016: Moderate Resolution Imaging Spectroradiometer (MODIS) MOD21 Land Surface Temperature and Emissivity Algorithm Theoretical Basis Document, http://hdl.handle.net/2014/45681

Hulley, G. C., S. J. Hook, E. Abbott, N. Malakar, T. Islam, and M. Abrams, 2015, The ASTER Global Emissivity Dataset (ASTER GED): Mapping Earth's emissivity at 100 meter spatial scale, *Geophys. Res. Lett.*, **42(19)**, pp. 7966-7976, doi: 10.1002/2015GL065564

Karnieli, A., N. Agam, R. T. Pinker, M. Anderson, M. L. Imhoff, G. G. Gutman, N. Panov, and A. Goldberg, 2010: Use of NDVI and Land Surface Temperature for Drought Assessment: Merits and Limitations. *J. Climate*, **23(3)**, pp. 618-633, doi:10.1175/2009JCLI2900.1

Li, Z., B. Tang, H. Wu, H. Ren, G. Yan, Z. Wan, I. F. Trigo, and J. A. Sobrino, 2013: Satellite-derived land surface temperature: current status and perspectives. *Remote Sens. Environ.*, **131**, pp. 14–37, doi: 10.1016/j.rse.2012.12.008

Liu, Y., Y. Yu, P. Yu, F. M. Göttsche, and I. F. Trigo, 2015: Quality Assessment of S-NPP VIIRS Land Surface Temperature Product. *Remote Sens.*, **7(9)**, pp. 12215-12241; doi: 10.3390/rs70912215

Liu, Y., Y. Yu, P. Yu, H. Wang, and Y. Rao, 2019: Enterprise LST Algorithm Development and Its Evaluation with NOAA 20 Data, *Remote Sens.*, **11(17)**, doi: 10.3390/rs11172003

McMillin, L. M., 1975: Estimation of sea surface temperatures from two infrared window measurements with different absorption, *J. Geophys. Res.*, **80(C36)**, pp. 5113–5117, doi: 10.1029/JC080i036p05113

McMillin, L. M. and D. S. Crosby, 1984: Theory and validation of multiple window sea surface temperature technique, *J. Geophys. Res.*, 89, pp. 3655-3661, doi: 10.1029/JC089iC03p03655

Meng, C. L., Z.-L. Li, X. Zhan, J. C. Shi, and C. Y. Liu, 2009: Land surface temperature data assimilation and its impact on evapotranspiration estimates from the common land model. *Water Res. Res.*, **45**, doi: 10.1029/2008WR006971

Menzel, W. P. and J. F. W. Purdom, 1994: Introducing GOES-I: The First of a New Generation of Geostationary Operational Environmental Satellites, *Bull. Amer. Meteor. Soc.*, **75**, pp. 757–781, doi: 10.1175/1520-0477(1994)075<0757:IGITFO>2.0.CO;2

Prata, A. J. and C. M. R. Platt, 1991: Land surface temperature measurements from the AVHRR, in Proc. 5th AVHRR Data Users Conf., Tromso, Norway, Jun. 25–28, pp. 438–443. EUM P09, 1991.

Prata, A. J., 1993: Land surface temperatures derived from the AVHRR and the ATSR, 1, Theory, *J. Geophys. Res.*, **98(D9)**, pp. 16,689–16,702, doi: 10.1029/93JD01206

Prata, A. J., 1995: Land surface temperatures derived from the AVHRR and the ATSR, 2, Experimental results and validation of AVHRR algorithms, *J. Geophys. Res.*, **99(D6)**, pp. 13,025–13,058, doi: 10.1029/94JD00409

Price, J. C., 1984: Land surface temperature measurements from the split window channels of the NOAA-7/AVHRR, *J. Geophys. Res.*, **89(D5)**, pp. 7231–7237, doi: 10.1029/JD089iD05p07231

Quintano, C., A. Fernández-Manso, L. Calvo, E. Marcos, and L. Valbuena, 2015: Land Surface Temperature as Potential Indicator of Burn Severity in Forest Mediterranean Ecosystems. *Int. J. Appl. Earth Obs.*, **36**, pp. 1-12, doi:10.1016/j.jag.2014.10.015

Schmit T. J., W. F. Feltz, W. P. Menzel, J. Jung, A. P. Noel, J. N. Heil, J. P. Nelso, and G. S. Wade, 2002: Validation and use of GOES sounder moisture information, *Wea. Forecasting*, **17**, pp. 139-154, doi: 10.1175/1520-0434(2002)017<0139:VAUOGS>2.0.CO;2

Schmit, T. J., P. Griffith, M. M. Gunshor, J. M. Daniels, S. J. Goodman, and W. J. Lebair, 2016: A Closer Look at the ABI on the GOES-R Series. *B. Am. Meteorol. Soc*., **98**, pp. 681-698, doi: 10.1175/BAMS-D-15-00230.1

Seemann, S.W., E. E. Borbas, R. O. Knuteson, G. R. Stephenson, and H.-L. Huang, 2008: Development of a Global Infrared Land Surface Emissivity Database for Application to Clear Sky Sounding Retrievals from Multi-spectral Satellite Radiance Measurements. *J. Appl. Meteor. Climatol.*, **47**, pp. 108-123, doi: 10.1175/2007JAMC1590.1

Sikorski, R. J., P. S. Kealy, and W. J. Emery, 2002: Land Surface Temperature Visible/Infrared Image radiometer Suite Algorithm Theoretical Basis Document, Version 5, Raytheon Systems Company.

Sobrino, J. A., Z. L. Li, M. P. Stoll, and F. Becker, 1993: Determination of the surface temperature from ATSR data, in *Proc. 25th Int. Symp. Remote Sens. Environ.*, Graz, Austria, Apr. 4–8, pp. II-19–II-109.

Sobrino, J. A., Z. L. Li, M. P. Stoll, and F. Becker, 1994: Improvements in the split-window technique for land surface temperature determination, *IEEE Trans. Geosci. Remote Sens.*, **32(2)**, pp. 243–253, doi: 10.1109/36.295038

Stenibrecht, W., H. Claude, U. Köhler, and K. P. Hoinka, 1998: Correlations between tropopause height and total ozone: Implications for long-term changes. *J. Geophys. Res.*, **103(D15)**, pp.19183-19192, doi: 10.1029/98JD01929

Sun, D. L., R. T. Pinker, and J. B. Basara, 2004: Land surface temperature estimation from the next generation of Geostationary Operational Environmental Satellites: GOES M-Q, *J. Appl. Meteorol.*, **43**, pp. 363-372, doi: 10.1175/1520-0450%282004%29043<0363%3ALSTEFT>2.0.CO%3B2

Trigo, I., S. Freitas, J. Bioucas-Dias, C. Barroso, I. Monteiro, and P. Viterbo, 2009 Algorithm Theoretical Basis Document for Land Surface Temperature (LST) Products: LSA-4(MLST)

Trigo I. F., S. Boussetta, P. Viterbo, G. Balsamo, A. Beljaars, and I. Sandu, Comparison of model land skin temperature with remotely sensed estimates and assessment of surface-atmosphere coupling ‚Journal of Geophysical Research Atmospheres, **120(23)**, pp. 12096-12111, doi: 10.1002/2015JD023812

Ulivieri, C. and G. Cannizzaro, 1985: Land surface temperature retrievals from satellite measurements, *Acta Astronaut.*, **12(12)**, pp. 977-985, doi: 10.1016/0094-5765(85)90026-8

Ulivieri, C., M. M. Castronouvo, R. Francioni, and A. Cardillo, 1994: A SW algorithm for estimating land surface temperature from satellites, *Adv. Space Res.*, **14(3)**, pp. 59–65, doi: 10.1016/0273-1177(94)90193-7

Vidal, A., 1991: Atmospheric and emissivity correction of land surface temperature measured from satellite using ground measurements or satellite data, *Int. J. Remote Sens.*, **12(12)**, pp. 2449–2460, doi: 10.1080/01431169108955279

Walton, C. C., W. G. Pichel, J. F. Sapper, and D. A. May, 1998: The development and operational application of non-linear algorithms for the measurement of sea surface temperatures with the NOAA polar-orbiting environmental satellites, *J. Geophys. Res.*, **103(C12)**, pp. 27 999–28 012, doi: 10.1029/98JC02370

Wan, Z. and J. Dozier, 1996: A generalized split-window algorithm for retrieving land-surface temperature measurement from space, *IEEE Trans. Geosci. Remote Sens*., **34(4)**, pp. 892–905, doi: 10.1109/36.508406

Wan, Z., 1999: MODIS Land-Surface Temperature Algorithm Basis Document (LST ATBD): version 3.3, (April 1999).

Wan, Z., P. Wang, and X. Li, 2004: Using MODIS Land Surface Temperature and Normalized Difference Vegetation Index Products for Monitoring Drought in the Southern Great Plains, USA, *Int. J. Remote Sens.*, **25(1)**, pp. 61-72, doi: 10.1080/0143116031000115328

Wan, Z., 2008: New refinements and validation of the MODIS Land-Surface Temperature/Emissivity products, *Remote Sens. Environ.*, **112(1)**, pp. 59–74, doi: 10.1016/j.rse.2006.06.026

Wan, Z., 2014: New refinements and validation of the collection-6 MODIS land-surface temperature/emissivity product, *Remote Sens. Environ.*, **140**, pp. 36-46. doi:10.1016/j.rse.2013.08.027

Wang, H., Y. Yu, P. Yu, and Y. Liu, 2019: Land Surface Emissivity Product for NOAA JPSS and GOES-R Missions: Methodology and Evaluation, *IEEE Trans. Geosci. Remote Sens.*, pp. 1-12, doi: 10.1109/TGRS.2019.2936297

Yu, Y., J. L. Privette, and A. C. Pinheiro, 2005: Analysis of the NPOESS VIIRS land surface temperature algorithm using MODIS data, *IEEE Trans. Geosci. Remote Sens.*, **43(10)**, pp. 2340–2350, doi: 10.1109/TGRS.2005.856114

Yu, Y., A. C. Pinheiro, and J. L. Privette, Correcting land surface temperature measurements for directional emissivity over 3-D structured vegetation, SPIE San Diego, July, 2006.

Yu, Y., J. P. Privette, and A. C. Pinheiro, 2008: Evaluation of split window land surface temperature algorithms for generating climate data records, *IEEE Trans. Geosci. Remote Sens.*, **46(1)**, pp. 179-192, doi: 10.1109/TGRS.2007.909097

Yu, Y., D. Tarpley, J. L. Privette, M. D. Goldberg, M. K. Rama Varna Raja, K. Y. Vinnikov, H. Xu, 2009(a): Developing algorithm for operational GOES-R land surface temperature product, *IEEE Trans. Geosci. Remote Sens.*, **47(**3), pp. 936-951, doi: 10.1109/TGRS.2008.2006180

Yu. Y., J. L. Privette, M. Goldberg, and D. Sun, 2009(b): Evaluation of the GOES land surface temperature algorithm using tower-based measurements from SURFRAD network, Proc., Second Conference on Earth Observation for Global Change, Chengdu, China.

Yu. Y., D. Tarpley, J. L. Privette, L. E. Flynn, H. Xu, M. Chen, K. Y. Vinnikov, D. Sun, and Y. Tian, 2012: Validation of GOES-R satellite land surface temperature algorithm using SURFRAD ground measurements and statistical estimates of error properties, *IEEE Trans. Geosci. Remote Sens.*, **50(3)**, pp. 704-713, doi: 10.1109/TGRS.2011.2162338

Zhang, D., R. Tang, W. Zhao, B. Tang, H. Wu, K. Shao, and Z. Li, 2014: Surface Soil Water Content Estimation from Thermal Remote Sensing based on the Temporal Variation of Land Surface Temperature. *Remote Sens.*, **6(4)**, 3170-3187, doi: 10.3390/rs6043170

Zheng, W., H. Wei, Z. Wang, X. Zeng, J. Meng, M. Ek, K. Mitchell, and J. Derber, 2012: Improvement of daytime land surface skin temperature over arid regions in the NCEP GFS

model and its impact on satellite data assimilation. *J. Geophys. Res.*, **117(D6)**, doi: 10.1029/2011JD015901

APPENDIX A The Baseline Algorithm

As of now, the baseline algorithm is the one being implemented in the ground system. Its details are provided as follows.

A.1 Processing Outline

The processing outline of the baseline LST is summarized in Figure A.1. The LST retrieval for each pixel is started by extracting ABI sensor datasets including brightness temperatures, solar-target-sensor geometry, pixel geolocation and the sensor data quality control flags. Following that, the process extracts ancillary datasets which can be categorized as ABI and non-ABI related datasets. The ABI related ancillary datasets include the ABI cloud mask and snow/ice mask, which are level 2 ABI products and are listed as dependency in Figure 3.1. While a snow/ice mask is required, it may be supplied either as ABI derived ancillary data, if available, or as non-ABI derived ancillary data with more details in the following section. Currently the ABI snow/ice product is the fractional snow coverage; from which the snow/ice mask can be derived, though a threshold is to be determined for such a derivation. The ABI land team is working with other algorithm teams on it since the snow/ice mask is widely required. The non-ABI related datasets include the land/sea mask, the emissivity, and the NCEP water vapor (WV). Note that ABI Emissivity product has been developing since 2009; the LST required emissivity input maybe switched as ABI related ancillary data. Note also that ABI may provide WV product with higher spatial resolution than the NCEP WV does. Once quality of the ABI WV product is validated, it should replace the NCEP WV as the input. In addition, algorithm coefficients and some processing control values are read in this step. Detail information on input datasets will be provided shortly in Algorithm Input sub-section. Next, the ancillary datasets (land/sea mask, snow/ice, emissivity and NCEP WV) are mapped to the ABI pixel location, and land checking process is performed to label each pixel with land/sea, inland water, snow/ice properties. Such ancillary data check information will be recorded in quality control flags of the LST data. Then, the ABI sensor data is filtered using the cloud mask for ensuring that only the cloud clear and probably clear pixels are processed for the LST retrieval. Before calculating LST for each cloudless and land masked pixel, day/night time flag is determined from the solar zenith angle of the sensor geometric data; and dry/moist atmospheric condition flag is determined using the NCEP water vapor information. LST of the pixel is calculated accordingly with the daytime/nighttime and dry/moist flags since the algorithm coefficients are stratified for the conditions. LST will be calculated for snow/ice pixels but indicated in the quality control flags. Meanwhile, flags of large view angle and very cold surface will be indicated for such pixels. Finally, the calculated LST values and their associated quality control flags, which were generated in each of the above steps, are combined with the LST product package and are written to files for user access.

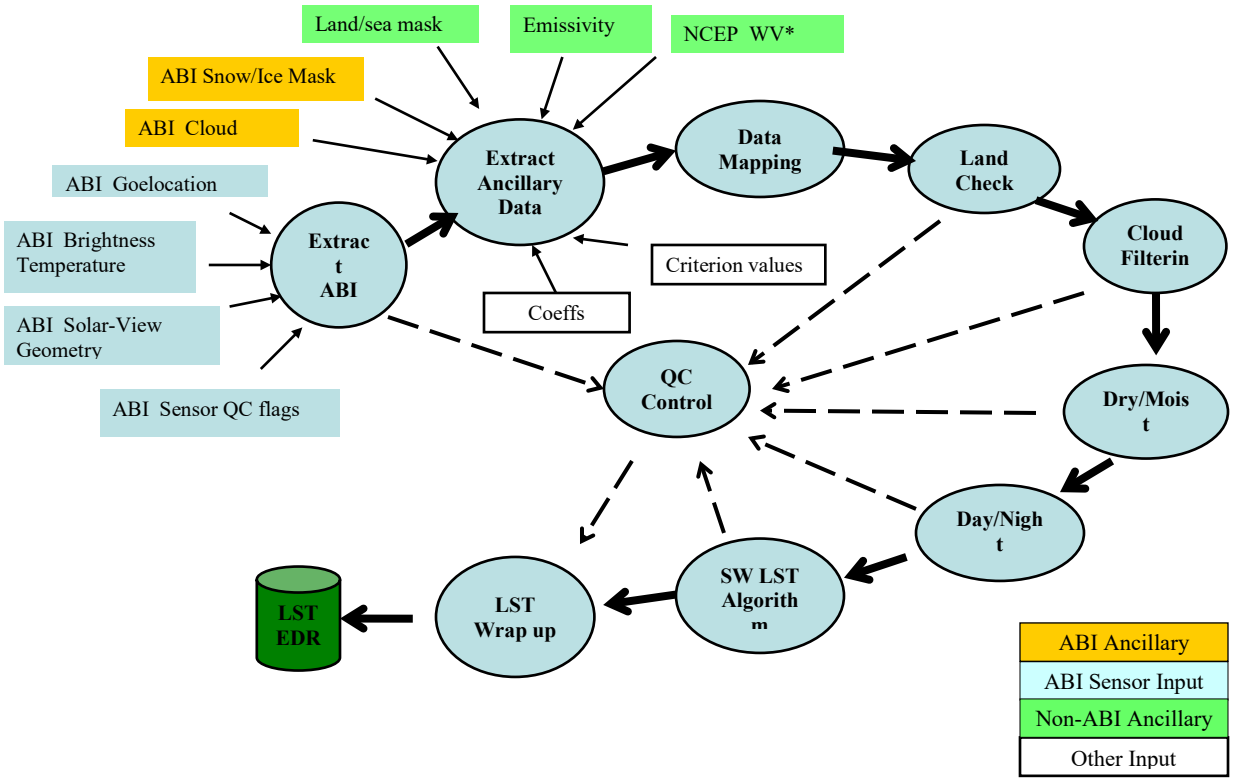

*The ABI WV data may replace the NCEP WV if its quality is verified.

Figure A.1. High Level Flowchart of the LST production for illustrating the main processing steps.

A.2 Algorithm Input

The primary sensor data, the derived sensor data, and the ancillary data for baseline LST retrieval are listed in Tables A.1, A.2, and A.3.

Table A.1. Input list of primary sensor data.

Name	Type	Description	Dimension	Unit
Ch14 brightness temperature	input	Calibrated ABI level 1b brightness temperatures at channel 14	grid (xsize, ysize)	Degree K
Ch15 brightness temperature	input	Calibrated ABI level 1b brightness temperatures at channel 15	grid (xsize, ysize)	Degree K
Latitude	input	Pixel latitude	grid (xsize, ysize)	Degree
Longitude	input	Pixel longitude	grid (xsize, ysize)	Degree
Solar zenith	input	ABI solar zenith angles	grid (xsize, ysize)	Degree
View zenith	input	ABI view zenith angle	grid (xsize, ysize)	Degree
QC flags	input	ABI quality control flags with level 1b data	grid (xsize, ysize)	Unitless

Table A.2. Input list of derived sensor data.

Name	Type	Description	Dimension	Unit
Cloud mask	input	ABI level 1cloud mask data	grid (xsize, ysize)	unitless
Snow/Ice mask	input	ABI level 2 Snow/Ice mask data	grid (xsize, ysize)	0-1.0 fraction of snow cover
Total Precipitable Water	input	ABI baseline TPW	grid (xsize, ysize)	mm
Land Surface Emissivity	input	ABI level 2 land surface emissivity	grid (xsize, ysize)	unitless

Table A.3 Input of ancillary data.

Name	Type	Description	Dimension
Land/sea mask	input	A land-ocean mask	grid (xsize, ysize)
Water vapor*	input	NCEP water vapor 6-hour forecast data	0.25 deg resolution
Emissivity*	input	MODIS monthly emissivity	0.05 deg resolution
IMS snow/ice mask*	input	Interactive multi-sensor snow and ice Mapping System	0.05 deg resolution

* Alternative input data in case the corresponding ABI product is not available at the GOES-R operation.

A.3 Algorithm Selection

Nine different algorithms (Table A.4) were selected as candidate algorithms for the ABI. Each algorithm consists of a "base" SW algorithm plus a path length correction. The base algorithms were adapted from the literature and represent a variety of formulations in terms of using the thermal infrared brightness temperatures and surface emissivity values. The path length correction, which is the last term in each algorithm, was added for additional atmospheric correction (Sikorski *et al.*, 2002; Walton *et al*., 1998). Geometric analysis shows that the atmospheric path length at 60^o of the satellite zenith angle is about 2 times larger than that at the nadir. Yu *et al*. (2008) showed that, if an algorithm's coefficients are determined for typical column water vapor amounts, algorithm accuracy can degrade significantly at large view angles unless a corrective term is applied. Therefore, we used the term, $(T_{11} - T_{12})(\sec\theta - 1)$, for path length correction. A detailed description of this term is in Yu *et al.* (2008).

Table A.4. Candidate split window LST algorithms. Each algorithm is composed of two parts: the base split window algorithm and path length correction (the last term in each algorithm). The base split window algorithms are adapted from those published split window algorithms as referred in the references, while the path length term is particularly added for additional atmospheric correction.

No	Formula[#]	Reference
1	$T_s = C + \left(A_1 + A_2\frac{1-\varepsilon}{\varepsilon} + A_3\frac{\Delta\varepsilon}{\varepsilon}\right)(T_{11}+T_{12}) + \left(A_4 + A_5\frac{1-\varepsilon}{\varepsilon} + A_6\frac{\Delta\varepsilon}{\varepsilon}\right)(T_{11}-T_{12}) + D(T_{11}-T_{12})(\sec\theta - 1)$	Wan & Dozier (1996); Becker & Li (1990).
2	$T_s = C + A_1\frac{T_{11}}{\varepsilon} + A_2\frac{T_{12}}{\varepsilon} + A_3\frac{1-\varepsilon}{\varepsilon} + D(T_{11}-T_{12})(\sec\theta - 1)$	Prata & Platt (1991); modified by Caselles *et al.* (1997).
3	$T_s = C + A_1T_{11} + A_2(T_{11}-T_{12}) + A_3(1-\varepsilon_{11}) + A_4\Delta\varepsilon + D(T_{11}-T_{12})(\sec\theta - 1)$	Coll & Valor (1997).
4	$T_s = C + A_1T_{11} + A_2(T_{11}-T_{12}) + A_3\frac{1-\varepsilon}{\varepsilon} + A_4\frac{\Delta\varepsilon}{\varepsilon^2} + D(T_{11}-T_{12})(\sec\theta - 1)$	Vidal (1991).
5	$T_s = C + A_1T_{11} + A_2(T_{11}-T_{12}) + A_3(T_{11}-T_{12})\varepsilon_{11} + A_4T_{12}\Delta\varepsilon + D(T_{11}-T_{12})(\sec\theta - 1)$	Price (1984).
6	$T_s = C + A_1T_{11} + A_2(T_{11}-T_{12}) + A_3\varepsilon + D(T_{11}-T_{12})(\sec\theta - 1)$	Ulivieri & Cannizzaro (1985).
7	$T_s = C + A_1T_{11} + A_2(T_{11}-T_{12}) + A_3\varepsilon + A_4\frac{\Delta\varepsilon}{\varepsilon} + D(T_{11}-T_{12})(\sec\theta - 1)$	Sobrino *et al.* (1994).
8	$T_s = C + A_1T_{11} + A_2(T_{11}-T_{12}) + A_3(1-\varepsilon) + A_4\Delta\varepsilon + D(T_{11}-T_{12})(\sec\theta - 1)$	Ulivieri *et al*. (1992).
9	$T_s = C + A_1T_{11} + A_2(T_{11}-T_{12}) + A_3(T_{11}-T_{12})^2 + A_4(1-\varepsilon_{11}) + A_5\Delta\varepsilon + D(T_{11}-T_{12})(\sec\theta - 1)$	Sobrino *et al.* (1993).

[#]Note:
T_{11} and T_{12} represent the top-of-atmosphere brightness temperatures of ABI channels 14 and 15, respectively;
$\varepsilon=(\varepsilon_{11}+\varepsilon_{12})/2$ and $\Delta\varepsilon=(\varepsilon_{11}-\varepsilon_{12})$, where ε_{11} and ε_{12} are the spectral emissivity values of the land surface at ABI channels 14 and 15, respectively;
θ is the satellite view zenith angle.
C, A_1, A_2, A_3, A_4, A_5, and A_6 are algorithm coefficients.

For each of the 9 algorithms, we calculated the bias and standard deviation of the regressions. Figure A.2 shows scatter plots of the regression results for the daytime dry atmosphere cases. It indicates that all algorithms perform well for an LST range from about 255 K to 305 K. The standard deviation (STD) of the differences between the prescribed LSTs and the retrieved LSTs

ranged from 0.35 K (algorithms 1, 3, 4, 7, 8, 9) to 0.47 K (algorithms 2 and 5). Similar accuracy is observed for the moist atmosphere cases, where the STD ranged from 0.65 K (algorithm 9) to 0.75 K (algorithms 2, 6). For the nighttime cases, similar regression accuracies are observed. STDs of the algorithms under different atmospheric conditions are listed in Table A.5.

Table A.5. Standard deviation errors (K) of the Regression analysis.

No	Daytime		Nighttime	
	Dry	Moist	Dry	Moist
1	0.35	0.70	0.32	0.92
2	0.47	0.75	0.47	0.96
3	0.35	0.70	0.33	0.92
4	0.35	0.70	0.32	0.92
5	0.47	0.72	0.47	0.94
6	0.46	0.75	0.45	0.95
7	0.35	0.70	0.33	0.92
8	0.35	0.70	0.33	0.92
9	0.35	0.65	0.31	0.89

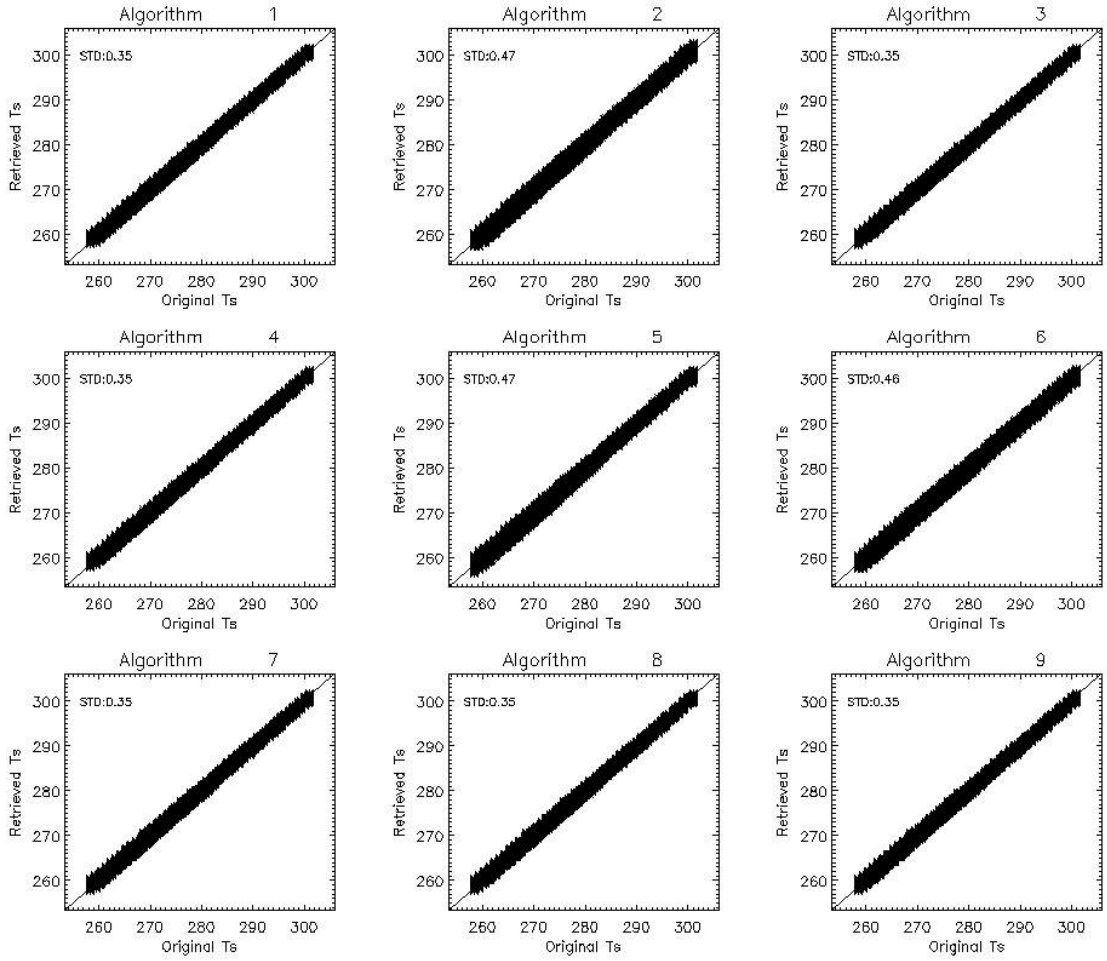

Figure A.2. Scattergram plots of the regression results for the dry atmosphere. Standard deviation (STD) errors of the regression are given in each plot (Daytime).

To have a closer look at error distributions, we produced histogram plots of the regression fits in Figures A.3-A.4 and Figures A.5-A.6 for daytime and nighttime results, respectively. Figures 3.10-3.13 reveal that there is no significant bias in any of the algorithms, and the error distributions are fairly symmetric (Gaussian-distribution-like) around zero. That means, all algorithms performed well and the retrieval noise level (less than 1.0 K) is smaller than the GS-F&PS requirement. Note that since the regression bias is zero for all the algorithms, the STD equals the accuracy of the regression statistics. We therefore used the STD as the accuracy metric in the simulation analyses.

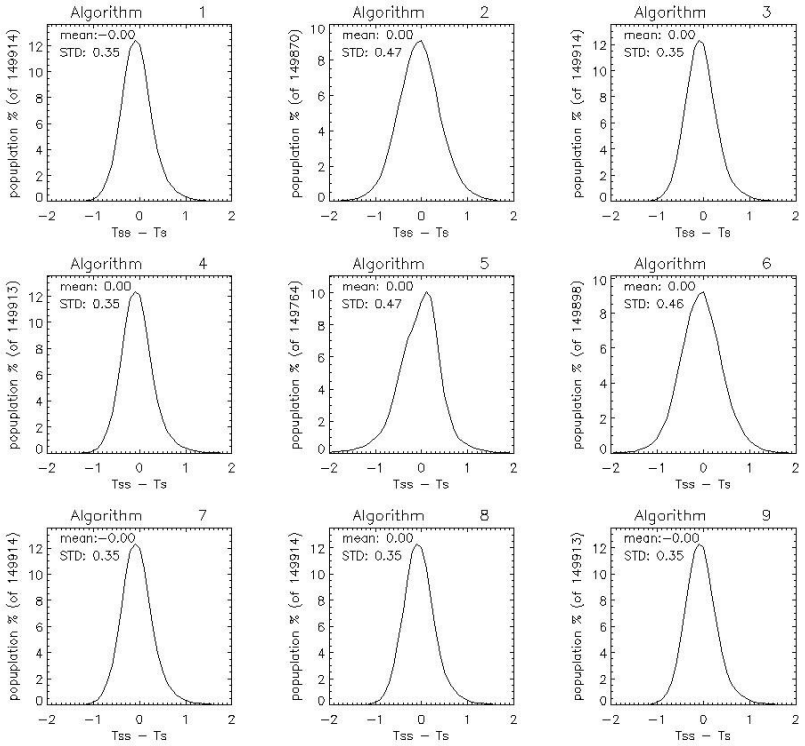

Figure A.3. Histogram plots of the regression results for the dry atmosphere (Daytime). Standard deviation (STD) and mean errors of the regression are given in each plot.

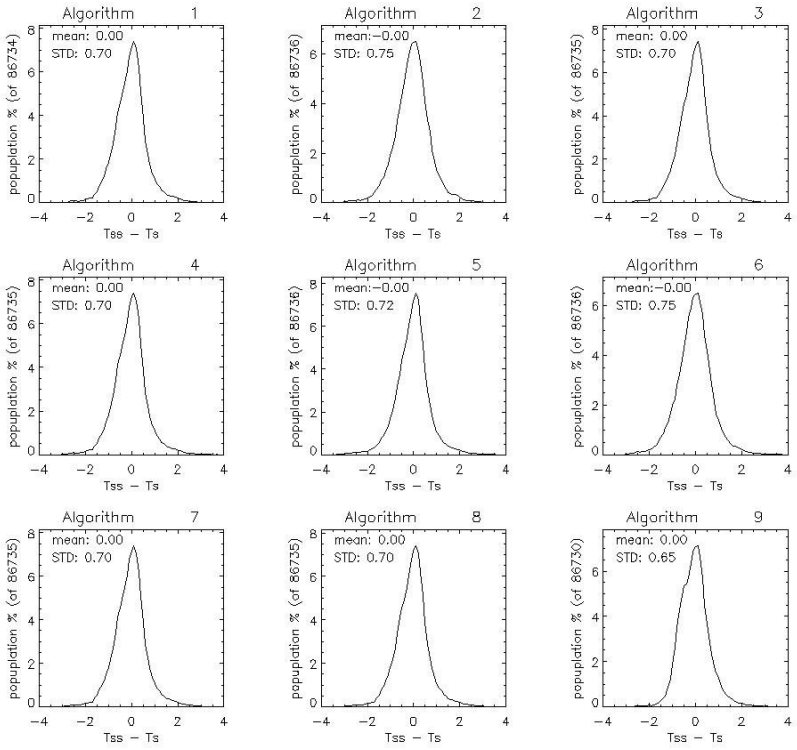

Figure A.4. Histogram plots of the regression results for the moist atmosphere (Daytime). Standard deviation (STD) and mean errors of the regression are given in each plot.

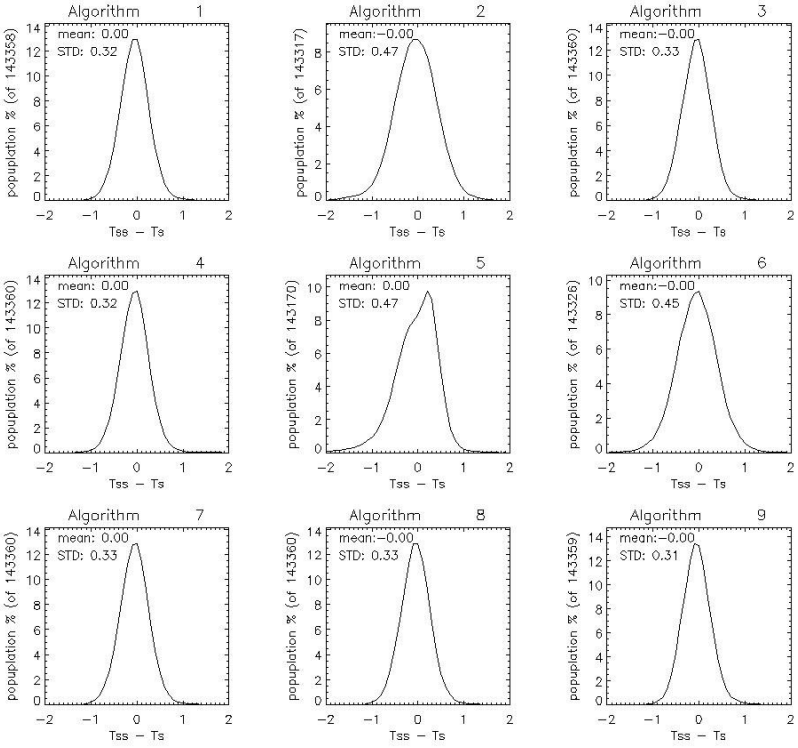

Figure A.5. Histogram plots of the regression results for the dry atmosphere (Nighttime). Standard deviation (STD) and mean errors of the regression are given in each plot.

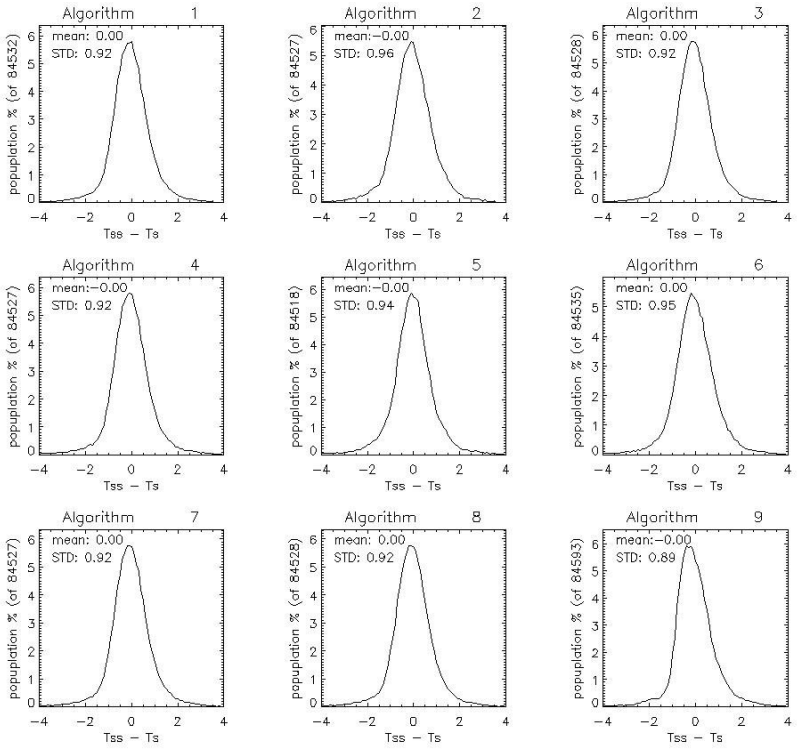

Figure A.6. Histogram plots of the regression results for the moist atmosphere (Nighttime). Standard deviation (STD) and mean errors of the regression are given in each plot.

Compared to the daytime algorithm performance, the standard deviation of the nighttime for the moist atmosphere cases is slightly worse for each algorithm. This is because the nighttime atmospheric profiles used in the simulation process are moister than the daytime atmospheric profiles. For the dry atmosphere cases, the regression standard deviation of each algorithm is similar between the daytime and the nighttime.

A.4 Variation and Uncertainty Estimation

Two important error sources in LST retrieval are the surface emissivity uncertainty and the atmospheric water vapor absorption. We therefore analyzed the sensitivities of the candidate LST algorithms (Table A.4) in terms of those two factors. The simulation dataset described above is used in the following estimations. The ABI LST retrieval algorithm will be determined from the results of the variation and uncertainty estimation.

A.4.1 Emissivity Uncertainty

Analytically, the maximum LST uncertainty δT_s due to the emissivity uncertainty can be described as,

$$\delta T_s = \sqrt{\delta T_1^2 + \delta T_2^2} \qquad \text{(A.1)}$$

where δT_1 and δT_2 represent the 11 and 12 micron band uncertainties resulting from the uncertainties of the mean emissivity (ε) and emissivity difference (Δε), respectively. Using algorithm 7 (Table A.4) as an example, these two components are

$$\delta T_1 = (A_3 - \frac{A_4}{\varepsilon^2})\delta\varepsilon \quad \text{and} \qquad \delta T_2 = \frac{A_4}{\varepsilon}\delta(\Delta\varepsilon) \tag{A.2}$$

Therefore, the maximum LST uncertainty for algorithm 7 is

$$\delta T_s = \sqrt{((\left(A_3 - \frac{A_4}{\varepsilon^2}\right)\delta\varepsilon)^2 + (\frac{A_4}{\varepsilon}\delta(\Delta\varepsilon))^2} \tag{A.3}$$

Considering $\varepsilon = (\varepsilon_{11} + \varepsilon_{12})/2$ and $\Delta\varepsilon = (\varepsilon_{11} - \varepsilon_{12})$, and assuming the emissivity uncertainties in each band are the same, *i.e.*, $\delta\varepsilon = \delta\varepsilon_{11} = \delta\varepsilon_{12}$, the maximum uncertainty of the emissivity difference is $\delta(\Delta\varepsilon) = |\delta\varepsilon_{11}| + |\delta\varepsilon_{12}| = 2\delta\varepsilon$. Thus, the LST uncertainty, δT_s, due to the emissivity uncertainty can be calculated using the above equation.

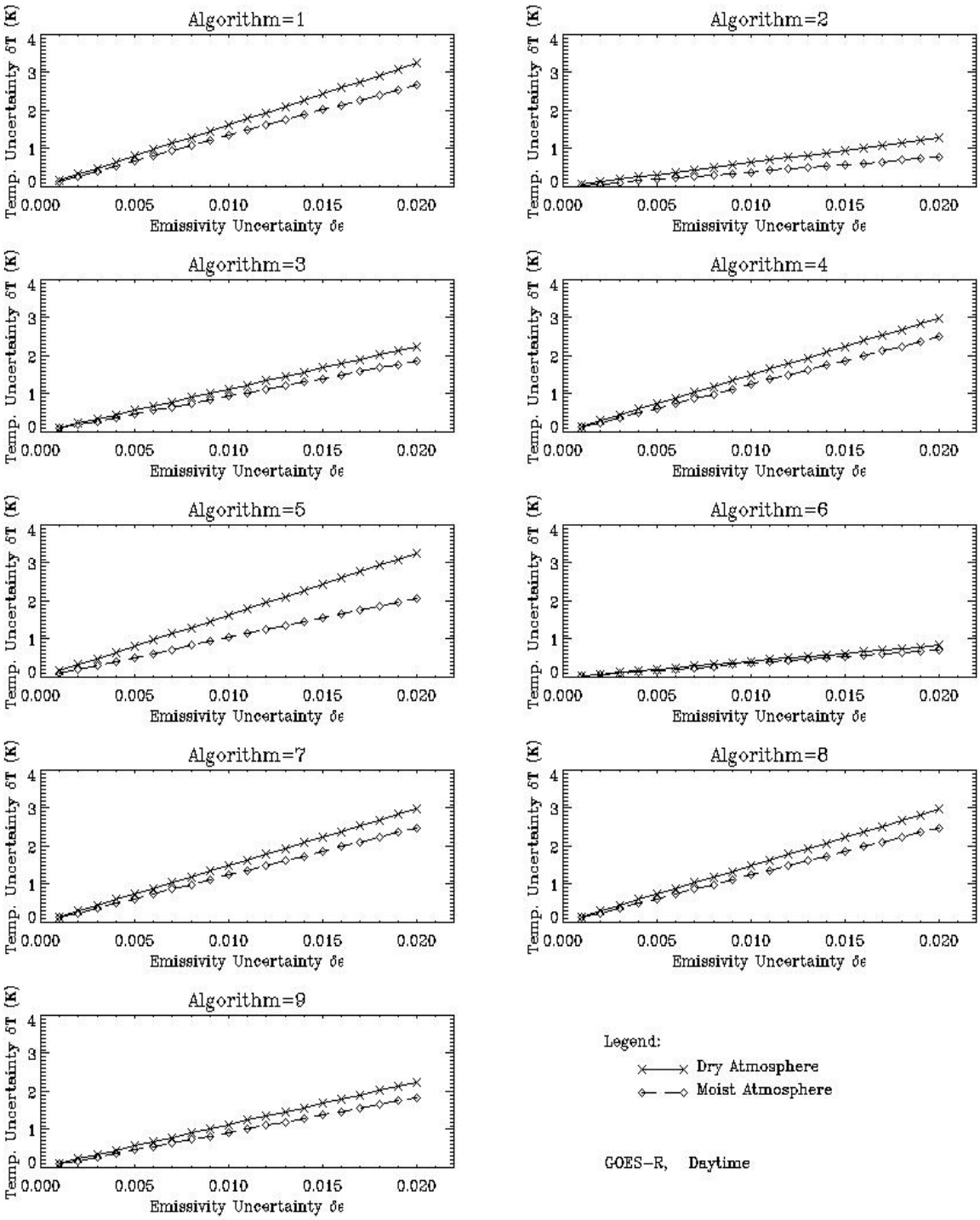

Figure A.7. Uncertainty of the retrieved LSTs along with the surface emissivity uncertainty for daytime algorithm. In the plots, it is assumed that mean emissivity ε=0.97, the emissivity difference Δε= 0.005 and the surface temperature is at about 298 K.

Emissivity sensitivities of the algorithms were estimated using equation (A.1), and are presented in Figure A.7, for the daytime case. For illustration purpose, we assumed that 1) the mean emissivity (ε) and emissivity difference (Δε) are 0.97 and 0.005, respectively, and 2) the

brightness temperatures are 295 K and 294 K for channels 14 and 15 of the ABI sensor, respectively. Results show that the LST uncertainty (δT) increases approximately linearly, and that uncertainty can be significant (up to 3 K) for fairly small uncertainty in emissivity. Thus, the algorithms are very sensitive to the emissivity error. Similar sensitivity results were observed for the nighttime cases, and therefore are not shown here. Note, however, that the predicted LST uncertainty calculated using equation (A.1) represents an extreme situation where all of the emissivity errors worsen the LST retrieval (i.e., the errors always compound rather than cancel each other). In practice, the final LST error may be significantly smaller, since emissivity errors at each channel may cancel each other and the temperature errors δT_1 and δT_2 may cancel each other.

In a relative sense, the sensitivity is lowest for algorithm 6, followed by algorithm 2. This is because, in algorithms 2 and 6, the emissivity difference ($\Delta\varepsilon$) is not used, and uncertainty of $\Delta\varepsilon$ can be double that of the mean emissivity. This implies that, to reduce the LST algorithm sensitivity to the emissivity error, the emissivity difference should not be included in the algorithm formulation. Note that emissivity sensitivity for the dry atmosphere is higher than that for the moist atmosphere since the LST algorithms for dry atmospheres are less affected by the atmospheric absorption and therefore are more accurate (Table A.5).

A.4.2 Water Vapor Uncertainty

Stratifying our regressions by water vapor regime, we assume that water vapor content can be well estimated *a priori*. In practice, water vapor information is usually available from satellite soundings, ground radiosondes and/or operational numerical weather prediction model forecasts. Nevertheless, two errors may occur. First, the water vapor value may be mis-measured due to a variety of error sources. Second, due to spatial resolution differences between the ABI data and water vapor data, both "dry" and "moist" atmospheric conditions may occur within the unit spatial area over which the water vapor was estimated (which may contain from several to more than ten GOES-R pixels). Therefore, the coefficient set of the LST algorithm for dry atmospheres may be incorrectly applied in a moist atmospheric condition, and vice-verse. To test the sensitivity of the algorithms to this error, we applied the algorithm coefficient sets derived for moist atmospheres to dry atmospheric conditions; and vice-versa.

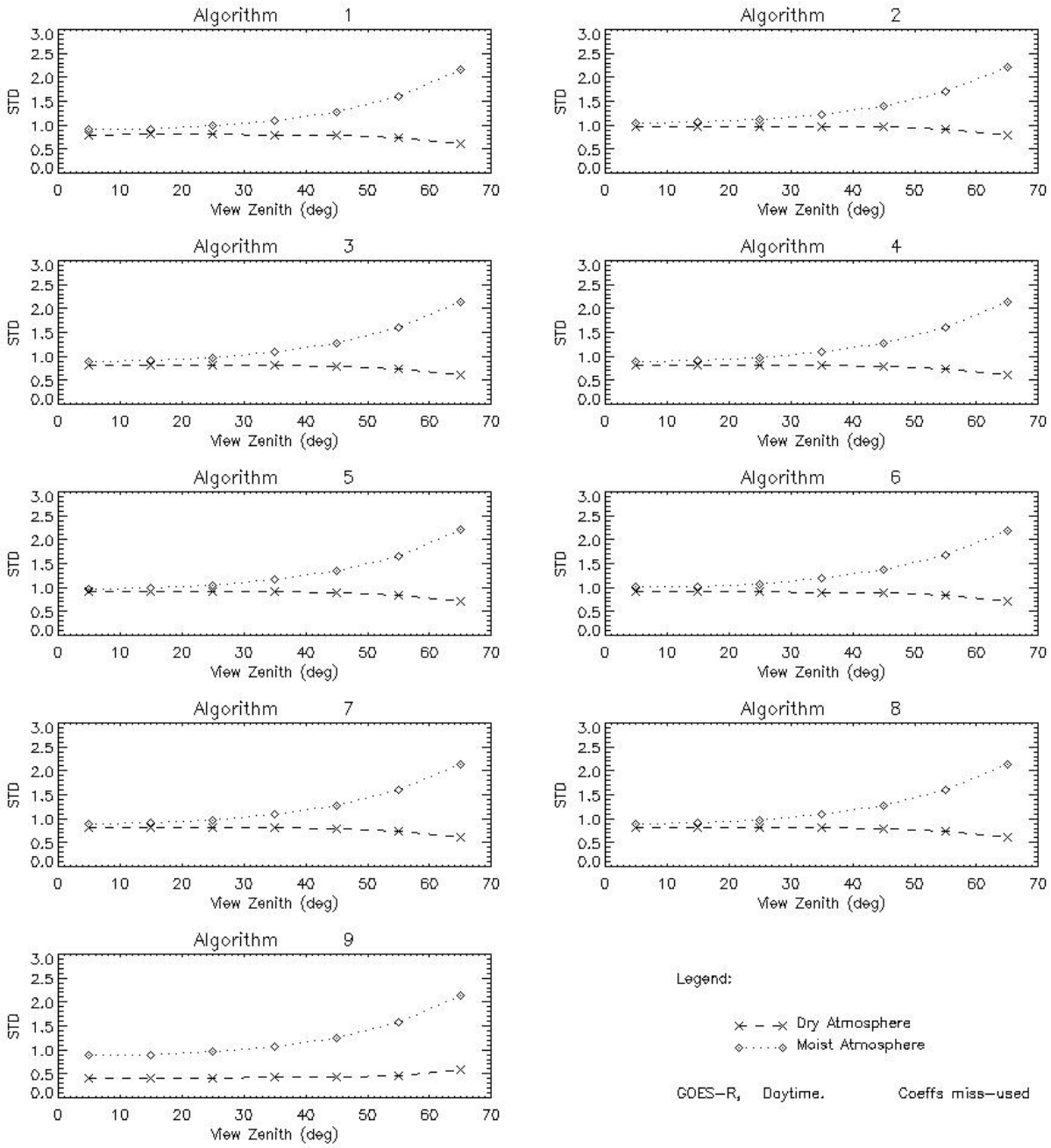

Figure A.8. Standard deviation errors when algorithm coefficients are wrongly applied (daytime cases). The dash lines (marked as Dry Atmosphere) represent the errors when the coefficients derived for moist atmosphere are applied for the dry atmospheric LST retrieval, while the dot lines (marked as Moist Atmosphere) represent the errors when the coefficients derived for dry atmosphere are applied for the moist atmospheric LST retrieval.

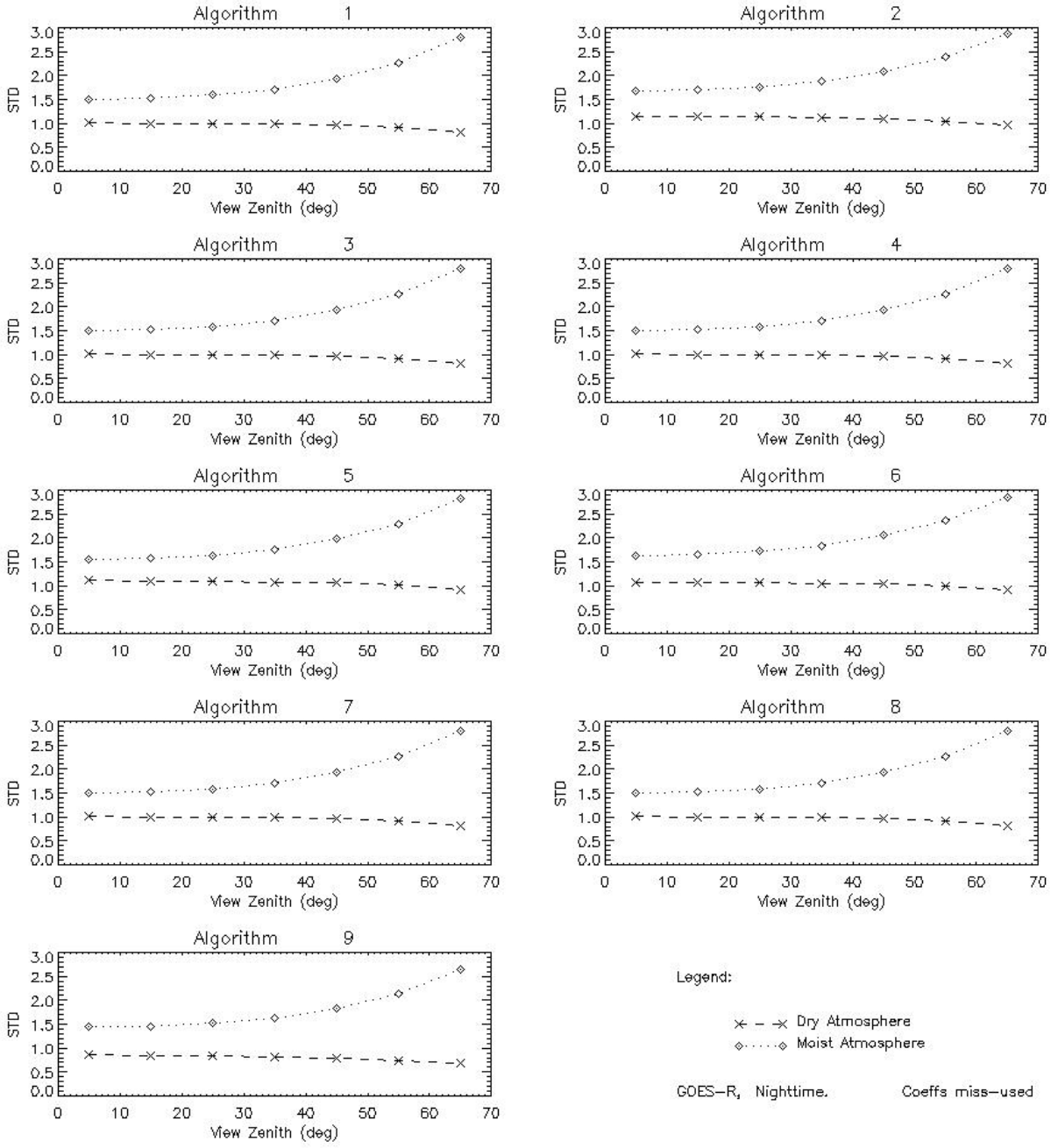

Figure A.9. Same as Figure A.8, except for the nighttime cases.

The water vapor sensitivity of the algorithms is illustrated for daytime and nighttime cases in Figures A.8 and A.9, respectively. In these cases, the STD is calculated separately in each 10-degree range of view zenith angles from 0 to 70 degrees. Note that, for all algorithms, the algorithm coefficients derived for dry atmospheric conditions are more sensitive if they are wrongly applied for the moist atmospheric conditions. This is particularly true for the nighttime cases since they are moister than the daytime cases. Further, for the moist atmospheric condition cases (the dot lines), such water vapor sensitivity increases when the satellite zenith angle increases. This is because the atmosphere is getting moister when the total column water vapor

along the view path increases with the increase of satellite zenith angle. For the dry atmospheric condition cases (the dash lines), the STD is significantly increased (comparing to the values in Table A.5), but it does not increase with the view zenith angle. In fact, the STD of the LST errors decreased (and is approaching the values of the moist atmospheric cases in Table A.5) when the zenith angle increases. This implies that even for the dry atmospheric conditions, the coefficient set for the moist atmospheric condition may be applicable when the satellite zenith angle is large.

A.4.3 Large Satellite View Angle

In addition, the GOES-R sensor view geometry may have significant impact on the variation of atmospheric absorption due to the radiative transfer path length increase from nadir to the edge of the scan. Considering that altitude of GOES-R satellite is about 36,000 km and the Earth radius is about 6700 km, the relationship between the satellite zenith angle (θ) and the satellite viewing angle (θ_v) is (Sun and Pinker, 2004)

$$\sin\theta = \frac{Satellite\ Altitude + Earth\ Radius}{Earth\ Radius}\sin\theta_v \approx 6.37\sin\theta_v \qquad (A.4)$$

Therefore, the maximum satellite viewing angle (about 8.7 degrees) corresponds to 74.48 degrees of view zenith angle. Such a large view zenith angle may have great impact on LST retrieval since, for instance, when the zenith angle is increased from 0 to 60 degrees, the atmospheric path length is doubled. We therefore assessed candidate algorithm sensitivity to the varying zenith angles using the simulation datasets.

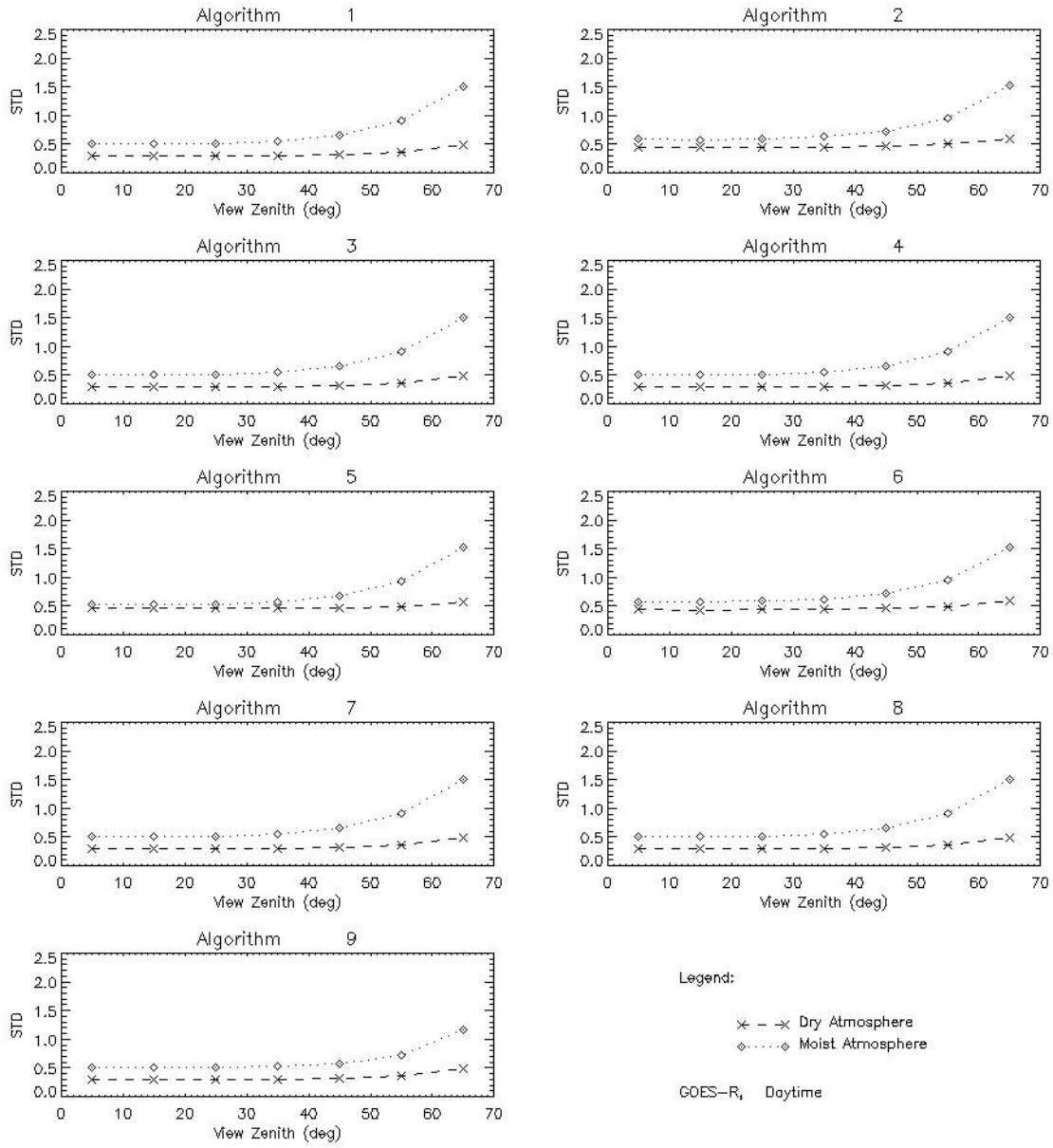

Figure A.10. Daytime algorithm standard deviation errors in different satellite view zenith angles.

The algorithm STD error distributions with satellite zenith angle are shown for the daytime cases in Figure A.10. It indicates that, for the moist atmospheric conditions, the STD error gets significantly worse when the zenith angle is larger than 45 degrees. For dry atmospheric conditions, the increase in STD is insignificant. Similar trends were observed for the nighttime cases (not shown).

Overall, similar water vapor sensitivity was found in all the algorithms, while algorithms 2 and 6 had significant smaller emissivity sensitivity than the other algorithms. Because simplicity is an advantage in operational procedures, algorithm 6 was chosen as the best candidate for further evaluation.

A.4.4 Summary of Algorithm Selection

We note that all algorithms listed in Table A.4 give similar retrieval accuracy. This primarily indicates the accuracy limitation of the current SW technique. The accuracy difference between the moist and dry atmospheric conditions implies that water vapor contamination is a major concern for the GOES-R LST retrieval. The largest errors are expected with SW algorithms when the atmosphere is moist and the satellite zenith angle is larger than 45 degrees. Accuracy of the retrieval under dry atmospheric conditions is significantly better than that under moist atmospheric conditions. Similar results were observed in Yu *et al.* (2008).

Emissivity sensitivity is a more serious problem. This is because the emissivity effect is coupled with the atmospheric absorption effect in the radiative transfer process; while the atmospheric absorption effect is linearized in the SW technique, the emissivity effect cannot be similarly linearized. A trade-off in current SW applications occurs since emissivity information improves retrieval accuracy, but inaccurate emissivity information may induce significant error. It is worth pointing out that the same conflict also occurs in all the SW LST algorithms, e.g., the LST algorithm developed for the NPP VIIRS sensors (Sikorski *et al*., 2002), that stratify the algorithm coefficients for different land surface types instead of using the emissivity information explicitly in the algorithm. For such algorithms, the emissivity uncertainty of a certain surface type may also induce significant LST retrieval error.

Our results demonstrate that, although using both the mean emissivity and the emissivity difference of the two thermal channels provide the best retrieval accuracy, such algorithms are too sensitive to the emissivity uncertainty and should not be used in operational practice. As a compromise, we recommend algorithm 6, which only requires the mean emissivity information, as the selected algorithm for generating the GOES-R LST product.

Finally, we emphasize that all the results discussed to this point assume perfect cloud detection. That is, all these results are for truly cloud clear pixels. Residual cloud effects in pixels detected as clear will add significant noise to the LST retrievals.

A.5 Algorithm Output

There are three LST products generated corresponding three ABI scan modes. As for the CONUS and Mesoscale modes, full resolution (i.e. 2 km) LSTs are produced. Output of the full resolution LST products mainly contains two data arrays: the LST values and associated product quality information (PQI) flags.
To minimize storage request of the LST product, the LST value is stored in a short integer using the following scaling equation:

$$T_{int} = T_s \times scaling\_factor - offset \qquad \text{(A.5)}$$

where T_{int} is the unsigned integer from the retrieved LST, T_s. User is directed to the product metadata for the scaling information.

The PQI flags are 2-byte bitwise short integer, which contains quality information of LST production for each pixel. In addition, a similar set of quality control (QC) flags is required for

operational monitoring purpose. The LST values and quality flags data arrays are described in Table A.6.

Table A.6. Algorithm output data.

Name	Type	Description	Dimension
LST values	Short Integer	Retrieved land surface temperature value for each pixel of the scanning mode.	grid (xsize, ysize)
Product Quality Information (PQI) flags	Short Integer	Bit-based product quality information for each pixel of the scanning mode: Land, cloudiness, sensor data quality, day/night, dry/moist, very moist, large view zenith, very cold surface, etc.	grid (xsize, ysize)
QC flags	Short Integer	Bit-based quality control flags for each pixel of the scanning mode	grid (xsize, ysize)

The product quality information flags may be comprised of a total of 16 bits holding the test results (yes/no) for each of the various tests and flags. Such PQI information is designed to help users in their applications. The quality control (QC) flags are solely related to the quality of the LST product, with 0 indicating good quality and 1 indicating problems associated with particular issues in the production and algorithm performance monitoring. Details of the LST PQI can be found in Table A.7 and the QC flags are defined in Table A.8.

Table A.7. Product quality information flags of the full resolution LST product.

Byte	Bit	Flag	Source	Effect
1	0-1	Empty		Reserved for future use
	2	Availability	SDR	00=normal, 01=out of space, 10=bad data, 11=missing data
	3			
	4	Surface Type	Land/sea Mask	00=land, 01=snow/ice, 10=in-land water, 11=sea
	5			
	6-7	Cloud Index	Cloud Mask	00=clear, 01=probably clear, 10=probably cloudy, 11=cloudy
2	0	Atmospheric Condition	LST	00=dry atmosphere (wv<=2.0g/cm^2); 01=moist atmosphere(wv>2.0g/cm^2); 10= very moist(wv>5.0/cm^2)
	1			
	2	Day/Night	SDR	0=day (solar zenith <= 85 deg), 1=night
	3	View Angle	LST	0=normal, 1=large view angle (LZA>55 deg)
	4	LST Quality	LST	00=normal, 01=cold surface (<250 K & >=213K), 10= out of range (not in 213-330K)
	5			
	6	Emissivity Quality	LST	0=normal, 1=historical emissivity
	7	Empty		Reserved for future use

Table A.8. Quality control flags of the full resolution LST product.

Byte	Bit	Flag	Source	Effect
1	0	Empty		Reserved for future use
	1	Availability	SDR	0=normal, 1=out of space, bad data, missing data
	2	Cloud Index	Cloud Mask	0=clear or probably clear, 1=probably cloudy, or cloudy
	3	View Angle	LST	0=normal, 1=large view angle (LZA>70°)
	4	Surface type	Land/sea mask	0 = land, including inland water, 1= water
	5	LST Quality	LST	0=normal, 1= out of range (not in 213-330K)
	6-7	Empty		Reserved for future use
2	0-7	Empty		Reserved for future use

The GOES-R AWG Algorithm integration Team (AIT) recommended that an overall quality flag (QF) is defined for simply indicating the data can be used (good) or not (bad).

In producing the Full Disk LST product, LST value, PQI and the QC flags described above are produced first for each original pixel (which is in 2 km resolution); an aggregation process is then applied over 5 by 5 pixels for generating the 10 km resolution Full Disk LST product if all of the 5 by 5 pixels are cloud free. The aggregated LST is the mean of the 25 pixels. Product quality information and quality control flags for the Full Disk LST product are similar to those for the CONUS and Mesoscale LST products, with a few redefinitions as shown in Table A.9 and Table A.10.

Table A.9. Product quality information flags of the Aggregated LST product.

Byte	Bit	Flag	Source	Effect
1	0-1	Empty		Reserved for future use
	2	Availability	SDR	00=normal, 01=out of space, 10=bad data, 11=missing data
	3			
	4	Surface Type*	Land/sea Mask	00=land, 01=snow/ice, 10=in-land water, 11=sea
	5			
	6-7	Cloud Index	Cloud Mask	00=clear, 01=probably clear, 10=probably cloudy, 11=cloudy
2	0	Atmospheric Condition*	LST	00=dry atmosphere (wv<=2.0g/cm^2); 01=moist atmosphere(wv>2.0g/cm^2); 10= very moist(wv>5.0/cm^2)
	1			
	2	Day/Night	SDR	0=day (solar zenith <= 85 deg), 1=night
	3	View Angle	LST	0=normal, 1=large view angle (LZA>55 deg)
	4	LST Quality*	LST	00=normal, 01=cold surface (<250 K & >=213K), 10= out of range (not in 213-330K)
	5			
	6	Emissivity Quality	LST	0=normal, 1=historical emissivity
	7	Empty		Reserved for future use

*Redefined for the Full Disk LST product only.

Table A.10. Quality control flags of the Aggregated LST product.

Byte	Bit	Flag	Source	Effect
1	0	Empty		Reserved for future use
	1	Availability	SDR	0=normal, 1=out of space, bad data, missing data
	2	Cloud Index	Cloud Mask	0=clear or probably clear, 1=probably cloudy, or cloudy
	3	View Angle*	LST	0=normal, 1=large view angle (LZA>70°)
	4	Surface type	Land/sea mask	0 = land, including inland water, 1= water
	5	LST Quality*	LST	0=normal, 1= out of range (not in 213-330K)
	6-7	Empty		Reserved for future use
2	0-7	Empty		Reserved for future use

*Redefined for the aggregated Full Disk LST product only.

In Table A.9, the largest flag value of the 5 by 5 pixels is assigned as the flag of the aggregated pixel for these flags: Availability, Cloud index, View angle, and Emissivity quality. The mixed pixel with Day and Night is flagged as Day.

As for the redefined flags, the mixed surface type (11) is for the pixel aggregated from land (00), snow/ice (01), and/or in-land water (10); the original sea flag is replaced. The mixed atmospheric condition (11) is defined as the mix of dry (00) and moist (01); one or more very moist pixels in the aggregation remain the very moist. For the LST quality, the aggregated pixel contains the normal and cold surface (or out of range) is flagged as cold (or out of range); or it is flagged as mixed if the cold surface and out of range occur in the containing pixels.

In addition to the pixel level LST values, PQI and quality control flags, metadata are needed in the LST product describing the common and LST specific information about the product. The GOES-R AWG and the Land Team recommend following metadata that (Table A.11) should be included in generating the ABI LST products.

Table A.11. Metadata defined for the LST product file.

METEDATA	TYPE	DEFINITOIN
DateTime	common	*Date and time of swath beginning and swath end*
Bounding Box	common	*Product resolution (nominal at nadir), number of rows and number of columns, byte per pixel, data type, byte order information, location of box relative to nadir (pixel space*)
Product Name	common	The ABI LST
Ancillary Data	common	*Ancillary data name used to produce the product: version number, origin (where it was produced), name*
Satellite	common	GOES-R
Instrument	common	Advanced Baseline Imager
Altitude	common	*Altitude of the satellit*e
Nadir	common	*Pixel in the fixed grid*
Position	common	*Latitude and longitude of the satellite positio*n
Projection	common	*Grid Projectio*n

Mode	common	*Type of Scan mode*
Version	common	*Product version number*
Compression	common	*Data compression type (method) used*
Location	common	*Location where the product is produced*
Contact	common	*Contact information of the producer/scientific supporter*
document	Common	*Citations to documents (i.e., ATBD*)
Number of PQI flag values	LST	8
For each PQI flag value, the following information is required: • Percent of retrievals with the PQI flag value • Definition of PQI flag		
Availability	LST	Valid ABI input excluding any pixel that is out of space, bad data, or missing data
Surface Type	Land/sea Mask	2-bit assigned, 00=land, 01=snow/ice, 10=in-land water, 11=sea
Cloud Index	Cloud Mask	2-bit assigned, 00=clear, 01=probably clear, 10=probably cloudy, 11=cloudy
Atmospheric Condition	LST	2-bit assigned, 00=dry atmosphere (wv<=2.0g/cm^2); 01=moist atmosphere(wv>2.0g/cm^2); 10= very moist(wv>5.0/cm^2)
Day/Night	SDR	0=day (solar zenith <= 85 deg), 1=night
View Angle	LST	0=normal, 1=large view angle (LZA>55 deg)
LST Quality	LST	2-bit assigned, 00=normal, 01=cold surface (<250 K & >=213K), 10= out of range (not in 213-330K)
Emissivity Quality	LST	0=normal, 1=historical emissivity
Number of QC flag values	LST	5
For each QC flag value, the following information is required: • Percent of retrievals with the QC flag value • Definition of QC flag		
Availability	LST	Valid ABI input excluding any pixel that is out of space, bad data, or missing data
Cloud Index	LST	Good if ACM indicates clear or probably clear, bad if ACM indicates probably cloudy, or cloudy
View Angle	LST	Good if LZA is less than 70°, bad if view angle is beyond product extent qualifier (LZA>70°)
Surface Type	LST	Good if land/sea mask indicates land or inland water, bad if it is water/ocean
LST Quality	LST	Valid range for LST product (213-330K)
Product Unit	LST	Degree Kelvin
Scaling Factor	LST	100
Offset	LST	10000

Statistics	LST	*Mean, minimum, maximum, and standard deviation of all the available LSTs*
Good pixels	LST	*Percentage of good LST retrieval (in range 230-330K*)
Total Pixels	LST	*Total pixels LSTs are retrieved (cloudless land surface pixels*)

Note: the definitions in *italic* words are determined at running.

It is noted that LST values will not be calculated for the pixels indicated as cloudy or probably cloudy, bad/out of space/missing data, ocean. Inland water pixel is considered as land pixel and the LST will be calculated over it.